FABRICATION OF CAPPED Ni-SiO_2 NANO-CATALYST AND STUDY OF ITS CATALYTIC EFFICACY TOWARD ORGANIC NITRO REDUCTION PROCESS

by

Keya Chowdhury

A THESIS SUBMITTED IN PARTIAL FULFILLMENT OF THE REQUIREMENT FOR THE DEGREE

OF

MASTER OF SCIENCE IN CHEMISTRY

Department of Chemistry

BANGLADESH UNIVERSITY OF ENGINEERING AND TECHNOLOGY (BUET)

DHAKA-1000, BANGLADESH.

April 2022

CANDIDATE'S DECLARATION

It is hereby declared that this thesis or any part of it has not been submitted elsewhere for the award of any degree or diploma.

Keya Chowdhury

(Keya Chowdhury)

Signature of the Candidate

Bangladesh University of Engineering and Technology (BUET), Dhaka-1000
Department of Chemistry

Certification of Thesis

A thesis on

FABRICATION OF CAPPED Ni-SiO_2 NANO-CATALYST AND STUDY OF ITS CATALYTIC EFFICACY TOWARD ORGANIC NITRO REDUCTION PROCESS

by

Keya Chowdhury

Roll No.: 1018032719F, Session: October-2018, has been accepted as satisfactory in partial fulfilment of the requirements for the degree of Master of Science (M.Sc.) in Chemistry and certify that the student has demonstrated satisfactory knowledge of the field covered by this thesis in an oral examination held on April 20, 2022

Board of Examiners

1. Dr. Al-Nakib Chowdhury
Professor
Department of Chemistry
BUET, Dhaka-1000.

Supervisor & Chairman

2. Dr. Md. Abdur Rashid
Professor and Head
Department of Chemistry
BUET, Dhaka-1000

Member (Ex-officio)

3. Dr. Ayesha Sharmin
Associate Professor
Department of Chemistry
BUET, Dhaka-1000

Member

4. Dr. Chanchal Kumar Roy
Assistant Professor
Department of Chemistry
BUET, Dhaka-1000

Member

5. Dr. Md. Mominul Islam
Professor
Department of Chemistry
University of Dhaka, Dhaka -1000

Member (External)

DEDICATED TO

MY FAMILY MEMBERS

AND

REVERENT TEACHERS

Table of Contents

List of Figures

List of Schemes

List of Tables

Acknowledgement

At first, I would like to thank Almighty for providing me with the physical and mental competence, patience, and bravery to complete the research work contained in this dissertation from the beginning of this program until now.

I would like to convey my profound gratitude to my respected supervisor, Dr. Al-Nakib Chowdhury, Professor, Department of Chemistry, BUET, for his kind supervision, invaluable assistance, insightful directives, and never-ending inspiration during my course work and research work. Without his guidance, persistent help, enthusiasm, dynamism, and motivation this dissertation would not have been possible.

I want to give special thanks Dr. Shakhawat Hossain Firoz Sir, Professor, Department of Chemistry, BUET for allowing to use his lab during my research.

I would like to express my gratitude to Dr. Chanchal Kumar Roy, Assistant Professor Department of Chemistry, BUET for his cordial support and suggestions during my research.

I want to give special thanks to our respected teacher Prof. Dr. Md. Abdur Rashid, Head of the Department of Chemistry, BUET for his support during the academic program. I am very thankful to all teacher of the Department of Chemistry at BUET, for their invaluable supports and guidance throughout the course and research. I would also like to thank all other officers and staffs of the Department of Chemistry, BUET.

I would like to express my deepest thanks and heartfelt gratitude to Md. Akter Hossain Reaz for his constant supports, suggestion, and technical guidance during my research work.

I would like to thank all senior and junior members of material research group and A.N.C research group for their supports during my research.

I am also grateful to CASR, BUET, Ministry of Science and Technology, Government of Bangladesh, and University Grants Commission (UGC) of Bangladesh for providing financial support for this research.

Finally, I would like to express my sincerest thanks to my family members for their continuous inspiration, moral supports, and immeasurable sacrifices during this project.

March 30, 2022

.....

(Keya Chowdhury)

Abstract

Immobilization of transition metal-based nano-catalysts with bio-based supports have gained desirable interest. Herein, SiO_2 nanoparticles from sugarcane bagasse (SCB) were utilized as a support to stabilize Ni NPs based nano-catalyst with different mass ratios (1:1, 1:2, and 1:3 of Ni and SiO_2) by a facile *in-situ* reduction in the presence of a capping agent CTAB. A capped nano silica powder was obtained by hydrolysis and condensation reaction from SCB ash using CTAB and sulfuric acid in a biphasic medium. Capped Ni-SiO_2 nano-catalyst has been prepared by the reduction of nickel(II) chloride using hydrazine hydrate, $N_2H_4.H_2O$ and sodium hydroxide, NaOH in the presence of capped SiO_2 NPs. FESEM, EDX, FTIR, and XRD analysis were employed to investigate the morphology and chemical nature of capped Ni-SiO_2 nano-catalysts. FESEM analysis revealed that spherical SiO_2 NPs with scattered pores and soft spongy suggested CTAB capping with an average diameter of 64 nm. It was also observed that Ni NPs have spherical particles with coral clusters with an average size of 54 nm. The FESEM of capped Ni-SiO_2 nano-catalyst demonstrated the Ni NPs were well-dispersed onto the surface of the SiO_2 NPs with the help of the capping agent CTAB with chain like nano-architectured. FTIR bands at 1060 cm^{-1} of capped Ni-SiO_2 nano-catalyst conformed the formation of Si-O-Ni bond. The EDX spectrum showed that Ni, O, and Si were uniformly distributed in the capped Ni-SiO_2 nano-catalyst. XRD patterns of the synthesized capped SiO_2 NPs formed an amorphous structure, whereas the Ni NPs and capped Ni-SiO_2 nano-catalysts formed face centered cubic (fcc) structures, indicating the purity and crystallinity of the samples. The catalytic activity of synthesized capped Ni-SiO_2 nano-catalyst with different mass ratio (1:1, 1:2, and 1:3 of Ni and SiO_2) was investigated utilizing UV-vis spectra to reduce 4-nitrophenol (4-NP) to 4-aminophenol (4-AP). The well-dispersed capped Ni-SiO_2 (1:2) nano-catalyst has shown a good catalytic performance. The rate constant *k*, activity parameter *K*, and turnover frequency (TOF) of the nano-catalyst are 0.2725 min^{-1}, 0.4087 mg^{-1} min^{-1}, and 0.1084 h^{-1}, respectively for capped Ni-SiO_2 (1:2) nano-catalyst. Moreover, capped Ni-SiO_2 nano catalyst has shown a good cycle stability and can achieve 89% 4-NP conversion to 4-AP even after 10 cycles.

Chapter-1

Introduction

1.1 General Introduction

Metal-based nanoparticles (MNPs) have obtained widespread attention because of their prospective applicability in optical, magnetic, energy storage devices and, most importantly, as a highly efficient catalyst [1, 2]. MNPs, existing as elements or composites, also have a broad functional diversity as nano-catalyst compared to bulk materials [1]. The catalytic reduction process has drawn high interest due to its high reactivity, selective chemical transformations with high product yields, tunability with ease of separation, and recyclability in recent years [3]. To enhance reduction efficacy, a wide range of materials like noble metals, transition metals, and even non-metal-based catalysts have been explored. However, much attention has required to the optimization and development of these nano-catalysts. For instance, various noble metals, such as Au, Ag, Pt, Au–Ag, and Au–Pt nano-catalysts, have been widely used due to their excellent catalytic activities, but their commercial use has been limited due to their high cost, complicated pathway to optimizes and limited resources [4]. To mitigate this impediment, transition metal-based nano-catalyst are rapidly gaining popularity for their noticeably lower cost and easy to handle than noble metal catalysts [5]. Among the various types of transition metal nanoparticles, nickel nanoparticles (Ni NPs) have attracted much attention because of their inexpensive, easy to access, mild reaction conditions and short time for high yields of products, magnetic properties, high catalytic activity, and rapid reaction with high selectivity as a catalyst in hydrogenation reactions [6]. The performance of Ni-based catalysts could be tied to their capability of absorbing hydrogen on the surface of Ni metal and quick activation of hydrogen in the atomic state [7]. Ni nanoparticles are also greener than the typical Raney® nickel catalyst [8]. However, the high surface energy and nano dimensional size of Ni NPs have extensively enhanced the particle agglomeration, which hindered their outstanding catalytic performance [9]. Supported nanoscale catalysts would be a good choice for Controlling the aggregation of Ni NPs with high dispersion, selective chemical conversions with high yields, easy separation, and recovery [10]. Several non-reactive materials such as alumina, metal oxides, zeolite, carbon nanotube, graphene, amorphous/crystalline SiO_2, amorphous carbon and various polymers have been numerously utilized as supports/stabilizers for ensuring the dispersion of Ni NPs to prevent agglomeration [11]. Among them, SiO_2 nanoparticles may be an alternative and excellent support candidate for their superior metal dispersion capabilities, high surface

area, pore structure, enhanced stability, and wettability [12, 13]. SiO_2 NPs could enhance the surface area significantly and thus appears to be an excellent support material in catalysis. However, some chemicals such as tetraethoxysilane and tetramethoxysilane are frequently employed as silica sources in the synthesis of nano-silica. These sources are relatively costly and have a high level of toxicity. The production of nano-silica materials from bio-waste, such as rice husk ash, bamboo leaves, sugarcane bagasse, and groundnut shell, has recently attracted the attention due to environmental and economic perspectives [14]. Sugarcane bagasse (SCB) has a great source of Silicon, recently attracted the attention of researchers for the synthesis of nano-silica materials SCB bio-waste based SiO_2 NPs is a promising candidate as supporting materials due to their low cost, abundant, facile, and ecofriendly, mesoporous structure, and large surface area [14]. Moreover, nanoporous SiO_2 NPs from SCB could be a potential solution to prevent aggregation of Ni NPs. Another possible solution to prevent aggregation and enhance stability, the Ni NPs was capped with SiO_2 NPs using a capping agent cetyltrimethylammonium bromide (CTAB). CTAB is a classical micelle maker and helps to control the size of nanoparticles and modify their surface [15]. The capping agents help to stabilize the interface between nanoparticles and their support surface. The specific structural features of nanoparticles are recognized to capping on their surface [16].

Therefore, nano-state catalysts would be employed to catalytically reduce the well-known toxic and environmentally hazardous nitroaromatics, converting them into harmless compounds before being released. 4-nitrophenol (4-NP), for example, is an impermeable pollutant found in industrial effluents and agricultural wastes that is harmful to human and animal organs such as the brain, liver, and kidneys [17]. Thus, it is becoming more and more important to remove 4-NP from an aqueous solution. Due to the slower effects of traditional approaches, it is essential to create new catalysts. A non-hazardous aromatic compound such as 4-AP is a potential intermediate to antipyretics medicine, dyestuff, corrosion inhibitors [18]. Traditionally, 4-aminophenol (4-AP) is synthesized using a multi-step iron-acid reduction of 4-NP to 4-AP, making major environmental issues due to producing a huge volume of Fe-FeO sludge. Additionally, Numerous studies have demonstrated the catalytic degradation of 4-NP. To address the ever-increasing demand for 4-AP, it is crucial to develop an

effective and environmentally friendly method for direct catalytic hydrogenation of 4-NP.

Herein, capped SiO_2 NPs has been prepared from a bio-based precursor SCB and utilized them as a support to immobilize Ni NPs in Ni-SiO_2 nano-catalyst using a facile *in-situ* chemical reduction in a controlled medium which employed to investigate its catalytical performance for nitroaromatics and to explore the catalytic mechanism. The results indicate that a facile technique for developing noble materials with high catalytic efficacy has been possible from affordable and locally available resources to turn hazardous materials into value-added goods.

1.2 Objectives of the Present Work

The main objectives of the present work include:

i. Synthesize Ni NPs by a simple chemical route and Preparation of capped SiO_2 NPs from sugarcane bagasse (SCB) bio-waste as well as fabricate capped Ni-SiO_2 nano-catalyst.
ii. Enhance the stability of the prepared nano-state particles by a capping agent (CTAB).
iii. Comprehend the morphological, structural, and compositional aspects of the capped Ni-SiO_2 nano-catalyst through FESEM, XRD, FTIR, EDX and UV-Vis analysis.
iv. Study the catalytic potential of the capped Ni-SiO_2 nano-catalyst toward nitro based organic compounds.
v. Propose a mechanism of reduction process of an organic compound using capped Ni-SiO_2 nano-catalyst.

1.3 Background

1.3.1 Nanoparticles

Since the preceding century, nanotechnology has been a well-known scientific topic. Nanoparticles (NPs) are a particulate compound ranging in size from one to one hundred nanometers [19]. Nanomaterials are unique for several reasons, one of which is their small size, as shown in Figure 1.1. Nanomaterials are 10000 times smaller than human hair and has a wide range of uses due to their tiny size. Their material properties alter as their size approaches the atomic scale. This is because the surface area to volume ratio has increased, causing the material's surface atoms to dominate its performance [20]. Because of their small size, nanoparticles have a substantially greater surface area to volume ratio than bulk materials such as powders, plates, and sheets [21].

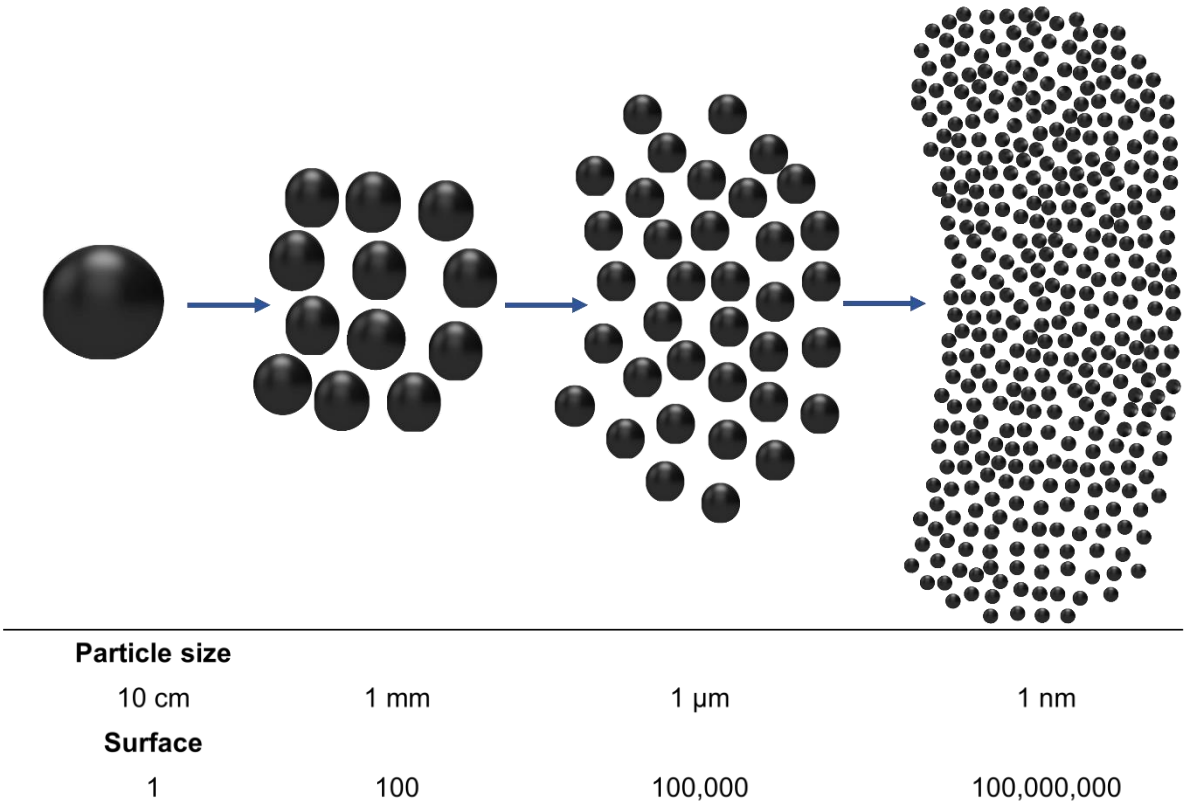

Figure 1.1: A schematic illustration of change in particle size from bulk to nano states.

Most significant and established pharmaceutical companies have internal drug delivery research programs that focus on formulations or dispersions with nanoscale components [22]. Antimicrobial treatments and dressings frequently contain colloidal silver [23]. Titania nanoparticle's strong reactivity, either on their own or when exposed with UV radiation, is also employed as filters for bactericidal applications [24]. Toxic poisons and other hazardous organic compounds are destroyed using enhanced catalytic characteristics of nano-ceramic or noble metal surfaces like platinum [25].

1.3.2 Metal-Based Nanoparticles

Metal nanoparticles (MNPs) are in high demand in the 21st century because of their physical and chemical differences from bulk metals and applications in different sectors. MNPs are composed entirely of the metal's precursors and have various features due to their well-known localized surface plasmon resonance characteristics, which has opened numerous pathways [26]. MNPs have unique characteristics over its bulk materials for instance (a) large surface energies, (b) compared to bulk, they have a large surface area to volume ratio, (c) quantum confinement, and (d) plasmon excitation. The surface to volume ratio of MNPs is higher, which allows them to interact with other particles easily [27]. For instance, MNP_S of alkali and noble metals such as Cu, Ag and Au have broad absorption bands in the visible region of the solar electromagnetic spectrum [28]. MNPs with regulated surface, size, and shape are significant in today's cutting-edge materials [29]. Due to their improved optical characteristics, MNPs are used in many research fields. For example, Au NPs are widely used for SEM sampling, which helps to obtain high-quality SEM images by improving electron flow [30].

1.3.3 Nano-catalyst

Nano-catalyst is a nanoparticle-based catalyst, draw a distinction between homogeneous and heterogeneous catalysts, offering advantages from both in terms of activity, selectivity, efficiency, and reusability in many circumstances [3]. For waste minimization, reduced energy consumption, and green conditions for chemical processes with improved efficiencies, it has recently been required to optimize the operating conditions and employ catalysts with improved activities, nano dimension, and selectivity [31]. Selectivity, highly activity, and reversibility of nano-catalyst gather lots of attention for a variety of approaches than its bulk [32]. The catalytic capabilities

of nano-catalysts are substantially reliant on numerous physical and chemical characteristics such as size, shape, content, and structure and may therefore be controlled and tuned. As a result, various nano-catalysts have exploded in the recent few decades, with significant advances in terms of activity, selectivity, and durability documented [32]. For example, Xu *et al* reported a novel graphene supported Cu@Ni bimetallic nanowires catalyst which was prepared *via* a facile liquid phase reduction method with good catalytic reduction applications of 4-NP to-AP [33]. Kang *et al* reported graphitic carbon embedded with Fe/Ni nano-catalysts from bacterial sources for efficient cracking of toluene [34]. Duan et al prepared a PdAuCu/C nano-catalyst for the reduction of 4-NP to 4-AP via controlling the deposition of noble metals [35].

A chemical reaction route consists of an active state and then products. A nano-catalyst is considered to generate a new activated complex with lower potential energy. Nano-catalyst provides an additional route with lower activation energy due to its high surface area and high surface to volume ratio. Consequently, the proportion of the total number of collisions with low activation energy increases, which means that the reaction rate also increases [36]. Figure 1.2 gives an energy diagram that depicts the nano-catalytic effect on the activation energy. It saves time and energy while achieving the same end results.

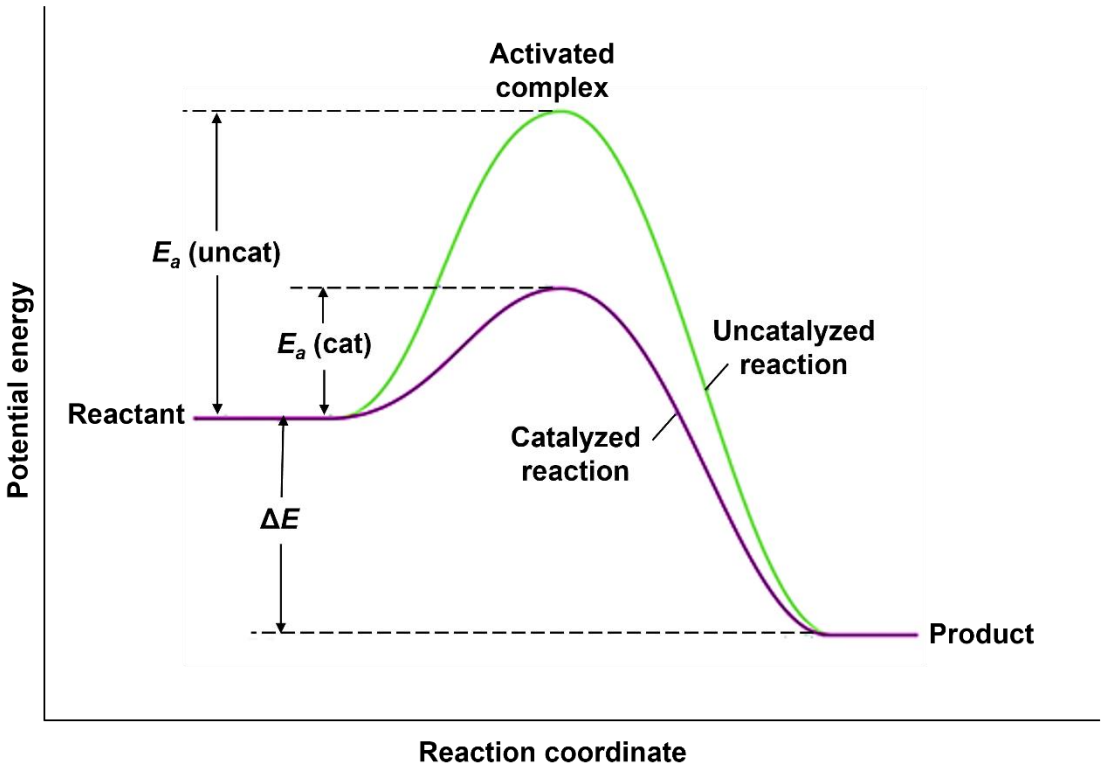

Figure 1.1: Energy profile diagrams of a process with and without catalyst.

1.3.3.1 Working Principles of Nano-catalysts

Although there is no uniform rule for defining a catalyst's activity, a nano-catalyst, in general, generates a whole new channel for the reaction in which the reactants are rapidly changed into products. In the presence of metal nano-catalysts, reactant molecules rapidly dissociate into atoms, even at low temperatures. One is reasonable

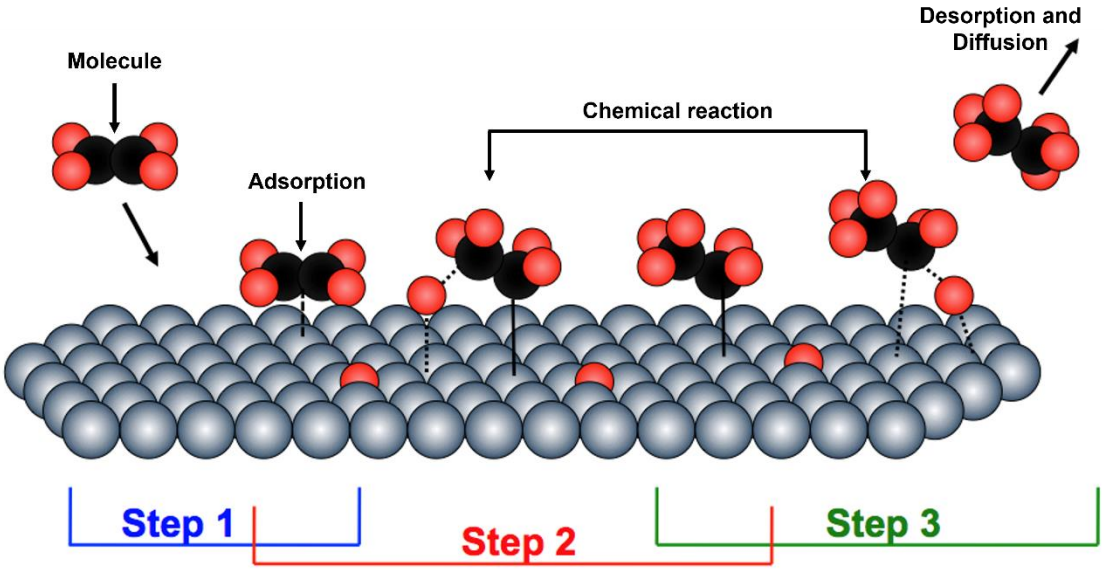

Figure 1.2: A molecular mechanism of a catalytic process on the nano-catalyst surface.

and simple explanation is summarized in Figure 1.3. The mechanism of heterogeneous nano-catalysis on the surface of solid catalysts consists of some steps. First, molecular reactants approach the metal surface and undergo physical adsorption with atoms' release by intermolecular forces [37]. Then, finally, break free from the surface, and the product molecules diffuse away from the surface [38].

1.3.3.2 Metal-based Nano-catalysts

Simple and efficient methods have been widely used to synthesize metal-based nano-catalysts in the past few years. These metal-based nano-catalysts may execute reactions due to their particular activity, stability, and porous structures [39]. Their increase and chemical composition may be managed by optimizing experimental situations to assemble exclusive shapes and designs. Metal-based nanomaterials containing high stability, controllable shape, and dispersibility have been manufactured for *in situ* and *ex-situ* applications. Thermal degradation, chemical reduction, and hydrothermal or

chemical precipitation methods are all used to make various kinds of nano-catalysts [40]. Furthermore, diatomite and ligands or capping agents can be used to generate nanoparticles with highly reactive surfaces. These nanoparticles are used as supported metal catalysts, metal oxide catalysts, core-shell structures, layered oxides, ceramic nano-catalysts, and other applications [41]. Transition metal-based nano-catalysts have been widely used in active catalytic applications because of their partially filled d-orbital. To promote the catalytic degradation of pendimethalin, a multifunctional recyclable catalyst comprised of polydopamine/Ag/polystyrene films was developed, and it has potential uses in the sectors of environmental protection, soil pollution remediation, and sewage treatment [42]. Recently, bimetallic silver/copper (Ag/Cu) nanoparticles synthesized using plant extracts have been demonstrated to remove chlorpyrifos efficiently [43]. Fe-, Pd-, Co-, and Ni-based nano-catalysts have also been utilized since they are less expensive and more readily accessible. For instance, silver nanoparticles, titanium oxides, doped titania, iron oxide nanoparticles, manganese oxides, aluminum oxides, titanium oxides, magnesium oxides, and cerium oxides have all been used for the formation of nano-catalysts due to short intraparticle diffusion, high reactive surface area, faster kinetics, and high adsorption with active reaction sites [42, 43]. Thus far, various bimetallic nanomaterials with improved activity, selectivity, and stability have been reported. Heterometallic nanostructures with precise composition, structure, size, and morphology have proven to be more effective tools for catalytic activity [44].

1.3.3.3 Noble Metal Nanoparticles as Nano-catalysts

Noble metal nanoparticles have attracted much interest because of their exceptional catalytic characteristics and are employed in various sectors, including environmental remediation, energy production, medical technology, and water treatment [42]. Environmental chemists have difficulty developing a simple and quick process for the degradation of organic dyes. Noble metal NPs, such as gold, silver, palladium, and platinum, have recently been employed to degrade different organic dyes [45]. For example, Pd nanoparticles can be used as catalysts for hydrogenation and alcohol oxidation in direct alcohol fuel cells [46]. The surface structure and electronic state of noble metal nanoparticles are affected by their size and shape, influencing their catalytic capabilities. The ratio of noble metal atoms on the surfaces, sides, and corners of nanoparticles is determined by the nanoparticle's size and shape, resulting in unique

catalytic activities for structure-sensitive reactions. For instance, Pt NPs was effectively used as a catalyst in the manufacture of organic substances [47, 48]. AuNPs based nano-catalyst have exhibited highly active catalytic characteristics, such as selective hydrogenation of organic molecules, carbon monoxide (CO) oxidation, and the water-gas shift reaction [49]. Noble metals have several disadvantages, including high cost, scarcity, and toxicity. It can be assumed that price is the main reason for this desire to move from precious metals [50]. Market factors tend to push the price of certain of these metals higher, especially due to the present global economic instability. High metal prices are a source of hardship for both companies and consumers, especially when considering the importance of catalysis in so many daily necessities, from medications to transportation.

1.3.3.4 Transition Metal Nanoparticles as Nano-catalysts

Recently, developing catalysts by employing low-cost, easily available materials has attracted huge attention rather than noble metals due to the low earth-abundant, cost and complicated processing routes of noble metals. Transition metal nanoparticles (TMNPs) are very attractive for use as catalysts due to their high surface-to-volume ratio, low cost, greenness, convenient use, and high surface energy [51]. TMNPs of Fe, Co, Ni, Cu, Ru, and Pd are effective catalysts because they can easily lend or absorb electrons from other molecules. The synthesis of different types of metal nanoparticles, such as Ni, Cu, and Fe, is comparatively difficult because they are easily oxidized [52]. Instead of employing other metal species, nickel nanoparticles (Ni NPs) have attracted much attention due to their unique properties with extreme stability [53-55]. In addition, Ni nanoparticles are more environmentally friendly than conventional Raney® nickel catalysts in that they create unwanted toxic waste [56]. It's worth noting that Ni NPs have superior physicochemical properties than bulk materials, which are more efficient in catalytic activity. The morphology of Ni-based nano-catalysts was reported to play a crucial role in determining the catalytic performances under thermally driven conditions [55, 56].

1.3.4 Supporting Materials for Nano-catalyst

MNPs usually trend to aggregate due to the high surface energy, which greatly limits their applications [57]. A support material with high surface area is required to prevent

their agglomeration and turn them into isolated MNPs [58]. The dispersion, size, and shape of the NPs have an impact on the catalytic performance. The activity of a MNPs catalyst is often increased by improving its dispersion on the support material, which enhances the active surface area of the catalysts. The composition and surface structure of the support material significantly impact the particle dispersion, size, and shape of MNPs. For instance, Ni NPs are well-known catalysts for hydrogenation of organic materials, and they have numerous physical and chemical advantageous features. Apart from the advantages of Ni NPs, one of the most difficult challenges in their application is preventing aggregation of Ni NPs. However, aggregation of Ni NPs can be handled by surface functionalization/stabilization or by using support-substances. Therefore, developing a novel approach is required to obtain finer Ni NPs with a high distribution. To stabilize MNPs, various support materials like silica (SiO_2) or alumina, zeolite, carbon nanotube, graphene, amorphous carbon, cellulose powder, polyamide, or polysaccharides are utilized. Figure 1.4 depicts the images of different stabilizers [59-60].

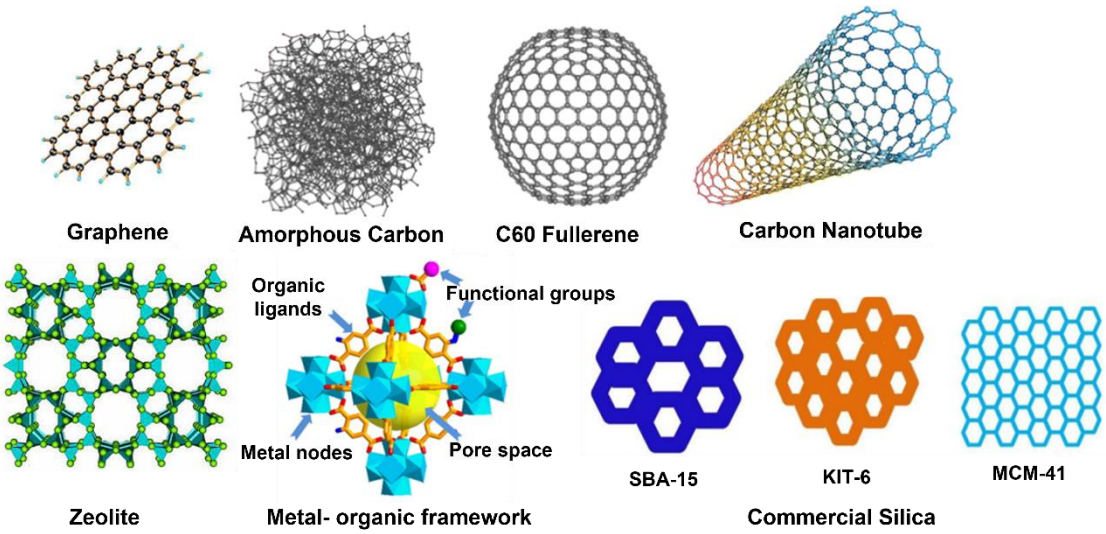

Figure 1.3: Important support materials popularly used in the synthesis of NPs [61, 62].

Among them, SiO_2 nanosphere have emerged as candidates for good supporting matrices because of their many Si-OH group surfaces, tunable porosity, biocompatibility, and functionality flexibility [63]. Virtually neutral character of SiO_2 based NPs as supported materials has great advantages. For example, to build SiO_2-supported copper catalysts for the dehydrogenation of ethanol to acetaldehyde compared to ZnO, Al_2O_3, and ZrO_2 support materials, SiO_2 nanosphere was utilized

[64]. On the other hand, undesirable side reactions of SiO_2 NPs support often lead to low selectivity. To improve selectivity, it is crucial to reduce or mask Si-OH on the SiO_2 surface by using a capping agent. This would improve the performance of SiO_2 nanosphere supported materials. Recently, another form of silica based supported material has attracted great attention [15]. For instance, amorphous SiO_2 NPs have demonstrated certain advantages in developing highly active supported catalysts due to their special physicochemical properties, such as high adsorption capacity [15]. Silica gel is another type of inorganic amorphous polymer of silicic acid made up of inters–linked SiO_4 units arranged in a tetrahedral pattern with oxygen as a binding site, resulting in the formation of silane bonds (Si–O–Si) and, eventually, nanometer-sized particles with the general formula SiO_2 [15]. The most common method for synthesizing silica is the sol-gel method. It is an easy, facile, and tunable method to prepare both MNPs supported silica NPs [65].

1.3.4.1 Bio-waste Supporting Materials

Nature functions as a vast "bio-laboratory," including plants, algae, fungi, yeast, and other biomolecule-based organisms. Bio-waste materials have been identified as an ecological burden, but they have inspired innovative possibilities for developing renewable, green, sustainable, low-cost, and long-term routes for nanomaterial synthesis [66]. Utilizing bio-based macromolecules as binding sources for the synthesis of NPs opens the new dimension of stabilizing and dispersing NPs to mitigate their aggregation. Naturally occurring biomolecules have a vital role in producing NPs of controlled shapes and sizes, which might be a greener, safer, and environmentally friendly protocol for synthesizing NPs [67]. It also helps to understand the health and safety consequences of NPs synthesis, as these routes eliminate the need to use toxic chemicals. For instance, to synthesize silica nanoparticles, some substances like tetraethoxysilane and tetramethoxysilane are widely utilized as silica sources [68]. However, these sources are relatively expensive and have a significant level of toxicity. Due to the high deposition of silica in agricultural residues, the production of nano-silica materials from bio-waste, such as rice husk ash, bamboo leaves, sugarcane bagasse, and groundnut shell, has recently attracted attention from an environmental and economic perspective [69]. Figure 1.5 shows the sugarcane bagasse and source of SiO_2. However, rice husk and ash are commonly cited in the literature as sustainable

sources for silicon-based value-added materials like SiO_2 NPs [70]. A few research studies have been conducted on using sugarcane bagasse (SCB) as a raw material to synthesize highly organized SiO_2 NPs [69]. Highly organized SiO_2 NPs have many applications in paints, biopolymers, membranes for fuel cells, catalysts, and adsorbents, among other applications [71]. Highly organized SiO_2 also acts as a support that can exhibit prospective advantages in the case of dispersion and preparation MNPs catalysts due to the higher ability of hydrogen production via enhancing the surface activities of NPs, high oxygen storage capacity, and high redox activity [72]. Therefore, a facile and scalable synthesis route of highly organized SiO2 based supports from SCB needs to be explored.

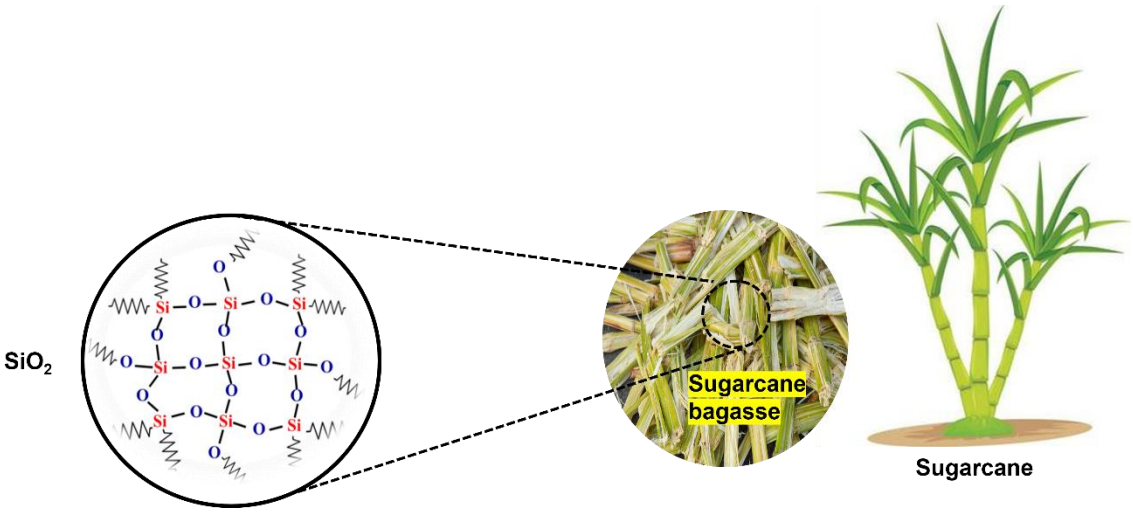

Figure 1.4: Schematic representation of sugarcane as one of the important silica sources.

1.3.5 Stability of Metal Nano-catalysts Using Capping Agent

NPs have a wide range of applications in various sectors, but due to their aggregation characteristics, their applications are limited. Because of their high surface energy of NPs usually causes extensive aggregation [73]. In various former methods capping agents have been utilized to obtain uniformly dispersed composite NPs. However, stabilizers and supporting materials have traditionally been used to create homogeneously distributed samples to overcome this difficulty [41]. As a result, using high surface area materials as supports for the fabrication of ultrafine and well-defined metal NPs that act as barriers to prevent encapsulated NPs from coalescing and improve

chemical and thermal stability and electrical conductivity of functional materials is a promising strategy. For example, e Au@Fe_3O_4–G and Pt@Fe_3O_4–G ternary hybrid nanomaterials exhibits excellent catalytic characteristics, and it can catalyze the reduction of 4-NP to 4-AP using $NaBH_4$ [74]. Polyol approach based on ethylene glycol was used to synthesize Ag nano cubes for the first time [75]. Citrate based substance are typically utilized as reducing agents for the syntheses of metal colloids which also serve as capping agents for the synthesis of different NPs [76]. Among various capping agents, a common surfactant, cetyltrimethylammonium bromide (CTAB), was extensively used in preparing rods, wires, and other shape nanoparticles [77]. CTAB is a cationic surfactant often used to make mesoporous silica nanoparticles. CTAB is formed micelle over the MNPs which helps to control the size of NPs, shape, prevent agglomeration, modify their surface, and surface functionality [14, 77].

1.3.6 Theories of Experimental Techniques

i. Fourier Transforms Infrared Analysis

Fourier transforms infrared (FTIR) spectroscopy is a well-established method for examining the chemical composition of smaller particles, generally 10 to 50 microns in diameter and larger regions on the surface [78]. FTIR spectroscopy works by measuring how the bonds of vibrating molecules absorb much light to produce a chemical fingerprint in the infrared part of the electromagnetic spectrum.

In FTIR spectroscopy, an interference wave interacts with the material instead of a dispersive instrument, where the interaction energy has a well-defined wavelength range. The interference wave is created in an interferometer (Figure 1.6), the most common of which is the Michelson interferometer. A computer controls the interferometer, which also collects and stores data and performs the Fourier transformation. The computer also handles post-spectroscopic procedures such as spectrum presentation, resolution enhancement, calibration, and correlation equation calculation [79]. The beam splitter divides a collimated light beam from the IR source directed to the Michelson interferometer. One half of the beam is reflected by a fixed mirror, while a moving mirror reflects the other half. After returning from the mirrors, the two light beams merge to form a reconstructed beam optically an interference wave. The interference light beam passes through the sample and changes its interaction with the sample. A deuterated triglycine sulfate (DTGS) pyroelectric detector often detects

the changing light. The analogue signals that arrive in the detector are digitized and stored in the computer via an analogue-digital-converter (ADC) [80]. Laser technology is required for a successful outcome in this technique. A laser beam suffers the same optical path modification as an IR beam in the interferometer. As a result, it can be used to reference the mirror's position during the scan. The laser beam also controls the collection of data points as a function of mirror movement [77].

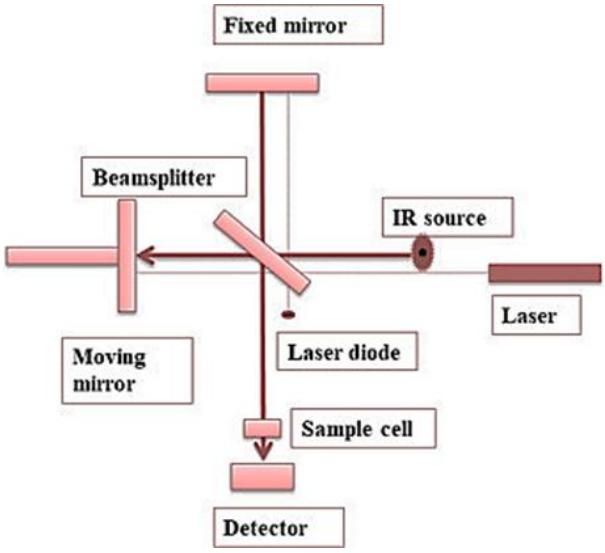

Figure 1.5: Schematic diagram of FTIR operation [79].

ii. X-ray Diffraction

Powder X-ray diffraction (XRD) was used to characterize crystalline properties, size, and phase identification using a RigakuD/maxTTRIII diffractometer. X-rays are created by a cathode ray tube, filtered to produce monochromatic radiation, collimated to concentrate, and directed toward the sample in these approaches. Constructive interference is created by the interaction of the incident light and the sample when conditions satisfy Bragg's Law which associates the wavelength of electromagnetic radiation with the diffraction angle and lattice spacing of the crystal sample. The X-ray's wavelength for diffraction ranges from about 0.5 to 2.5 Å [82].

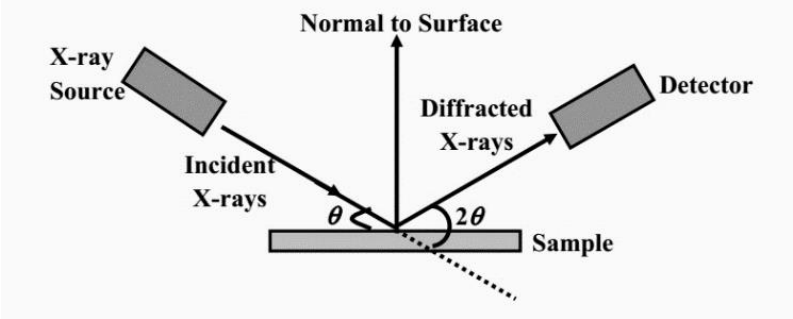

Figure 1.6: Schematic representation on the working principles of X-ray diffraction [81].

By scanning the sample through a range of 2θ angles, all possible lattice diffraction directions are obtained due to the random orientation of the powdered material. Because each material has its set of *d*-spacing, converting the diffraction peaks to d-spacing enables the substance to be recognized. Bragg's law [81] is used to calculate the value of d- spacing, as shown in Figure 1.7**.**

$$2d\ sin\ \theta = n\lambda \qquad [1]$$

where "d" is interlayer spacing, "θ" is the x-ray angle of incidence (and of diffraction) measured concerning the crystalline planes, "n" is an integer value and "λ" is the wavelength of the incident beam. XRD provides precise information about the lattice parameter, lattice defects, lattice strain, crystallite size (in case of nanoparticles) and the type of molecular bond of the crystalline phase. The Scherrer formula is used to calculate crystallite size [83].

$$D = k\lambda / \beta\ cos\ \theta \qquad [2]$$

where "*D*" is the crystallite size, *k* is a dimensionless shape factor (typical value 0.9), "λ" is the x-ray wavelength, "β" is the line broadening at halfway of the maximum intensity (FWHM) and θ is the Bragg angle (in degrees) [82].

iii. Field Emission Scanning Electron Microscope

The Field Emission Scanning Electron Microscope (FESEM) is a powerful modern technology for material characterization that reveals the surface morphology (texture), crystalline structure, and orientation of the components that comprise the sample [84]. The FESEM is a microscope that uses electrons with a negative charge rather than light. A field emission source produces these electrons. The material is scanned with electrons

in a zig-zag pattern, as shown in Figure 1.8. After being discharged from a field emission source, electrons are propelled in a high electrical field gradient. Electronic lenses within the high vacuum column focus and deflect these so-called primary electrons, resulting in a narrow scan beam that bombards the material. Secondary electrons are emitted from each point on the object as a result. The surface structure of the item influences the angle and velocity of these secondary electrons. The secondary electrons are captured by a detector, which generates an electrical signal [85].

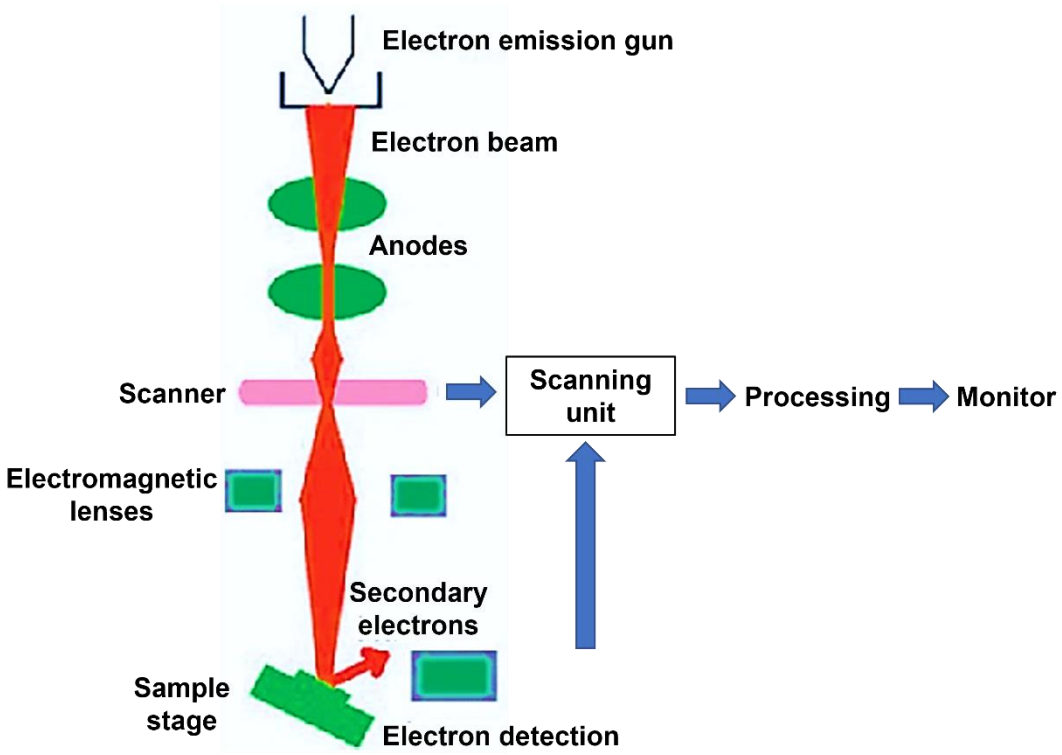

Figure 1.7: A schematic illustrations of field emission scanning electron microscope modules and operation process [85].

This signal is amplified and converted to a monitor or digital image, which may then be saved and processed. In most situations, data are gathered across a specific region of the material's surface, a 2-dimensional black and white image displaying spatial changes in these attributes is created. In a scanning mode, FESEM methods can photograph regions ranging in width from 1 cm to 5 microns (magnification ranging from 20X to approximately 500000X, the spatial resolution of 50 to 100 nm).

iv. Energy Dispersive X-ray Spectroscopy

Energy dispersive X-ray (EDX) spectroscopy is a microanalysis technique used to determine material's elemental composition and chemical characterization [86]. Because of its imaging capabilities, this equipment is frequently used in combination with an electron microscope, such as a SEM or TEM [87].

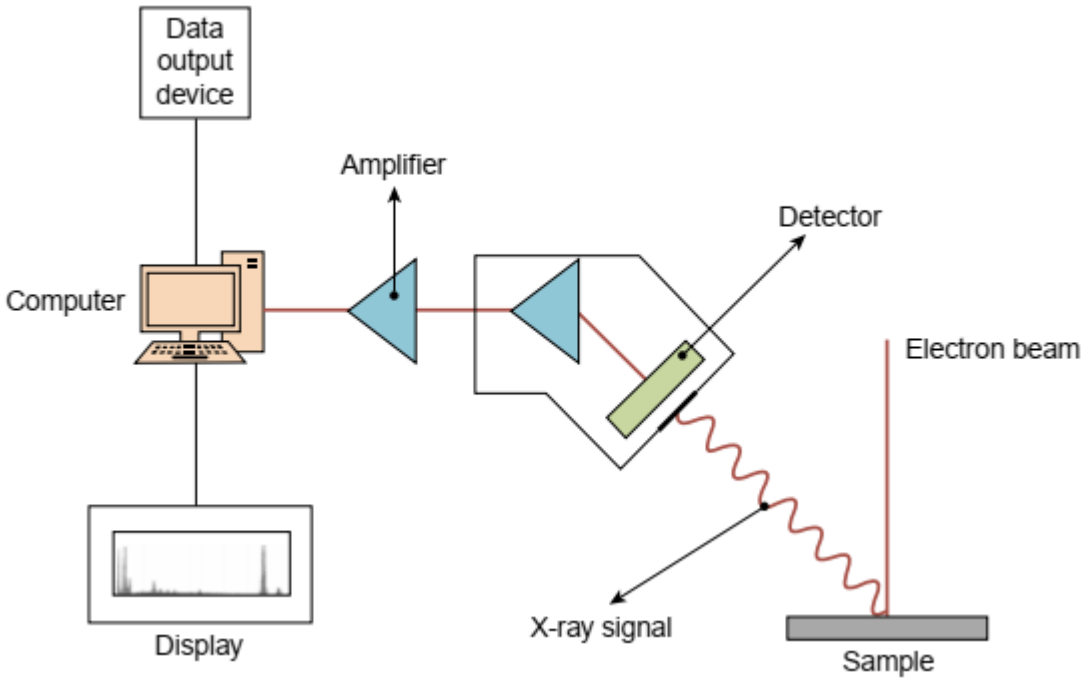

Figure 1.8: Operational modes of energy dispersive X-ray spectroscopy [87].

The bombardment of the electron beam of SEM ejects electrons from the sample's atoms comprising the sample's surface. As a result, electron vacancies are filled by electrons from a higher state, and an x-ray is released to compensate for the energy difference between the vacant and filled states. These X-rays can be detected by a detector calibrated for cobalt metal emission (6.925 keV) and then utilized to identify and analyze the elemental composition and abundance of the specimen surface [88]. The numerous emission lines associated with X-rays emitted from an atom are called after the shell of the original vacancy, for example, K, L, M, and so on. The shell of the electron that fills the gap is denoted by the Greek character with subscript. With the use of supporting software, one may acquire a full elemental spectrum and easily detect peaks, making EDX a great survey tool for swiftly identifying unknown phases prior to quantitative investigation. In semi-quantitative mode, EDX can be used to identify chemical composition using a peak-height ratio relative to a standard [86, 88].

1.4 References

[1] Wu, X., Xing, W., Zhang, L., Zhuo, S., Zhou, J., Wang, G., and Qiao, S., "Nickel Nanoparticles Prepared by Hydrazine Hydrate Reduction and Their Application in Supercapacitor," *Powder Technol.,* vol. 224, pp. 162-167, 2012.

[2] Javaid, S., Farrukh, M. A., Muneer, I., Shahid, M., Khaleeq-ur-Rahman, M., and Umar, A. A., "Influence of Optical Band Gap and Particle Size on the Catalytic Properties of $Sn/SnO_2–TiO_2$ Nanoparticles," *Superlattices Microstruct.,* vol. 82, pp. 234-247, 2015.

[3] Hu, H., Xin, J. H., Hu, H., Wang, X., Miao, D., and Liu, Y., "Synthesis and Stabilization of Metal Nanocatalysts for Reduction Reactions – a Review," *J. Mater. Chem. A,* vol. 3, pp. 11157-11182, 2015.

[4] Li, B. and Xu, Z., "A Nonmetal Catalyst for Molecular Hydrogen Activation with Comparable Catalytic Hydrogenation Capability to Noble Metal Catalyst," *J. Am. Chem. Soc.,* vol. 131, pp. 16380-2, 2009.

[5] Senapati, S., Srivastava, S. K., Singh, S. B., and Mishra, H. N., "Magnetic Ni/Ag Core–Shell Nanostructure from Prickly Ni Nanowire Precursor and Its Catalytic and Antibacterial Activity," *J. Mater. Chem.,* vol. 22, 2012.

[6] Jiang, H.-y., Zhang, S.-s., and Sun, B., "Highly Selective Hydrogenation with Ionic Liquid Stabilized Nickel Nanoparticles," *Catal. Lett.,* vol. 148, pp. 1336-1344, 2018.

[7] Alonso, F., Riente, P., and Yus, M., "Hydrogen-Transfer Reduction of Carbonyl Compounds Catalysed by Nickel Nanoparticles," *Tetrahedron Lett.,* vol. 49, pp. 1939-1942, 2008.

[8] Du, Y., Chen, H., Chen, R., and Xu, N., "Synthesis of P-Aminophenol from P-Nitrophenol over Nano-Sized Nickel Catalysts," *Appl.Cat. A: General,* vol. 277, pp. 259-264, 2004.

[9] Tian, Y., Liu, Y., Pang, F., Wang, F., and Zhang, X., "Green Synthesis of Nanostructed Ni-Reduced Graphene Oxide Hybrids and Their Application for Catalytic Reduction of 4-Nitrophenol," *Colloids and Surfaces A: Physicochem. and Engineer. Aspects,* vol. 464, pp. 96-103, 2015.

[10] LaGrow, A. P., Ingham, B., Toney, M. F., and Tilley, R. D., "Effect of Surfactant Concentration and Aggregation on the Growth Kinetics of Nickel Nanoparticles," *J. Phys.Chem. C,* vol. 117, pp. 16709-16718, 2013.

[11] Zhai, Y., Dou, Y., Liu, X., Park, S. S., Ha, C.-S., and Zhao, D., "Soft-Template Synthesis of Ordered Mesoporous Carbon/Nanoparticle Nickel Composites with a High Surface Area," *Carbon*, vol. 49, pp. 545-555, 2011.

[12] Wang, K., Zhang, Y., Zhao, J., Yan, C., Wei, Y., Meng, M., Dai, X., Li, C., and Yan, Y., "Facile Synthesis of Hierarchical Porous Solid Catalysts with Acid–Base Bifunctional Active Sites for the Conversion of Cellulose to 5-Hydroxymethylfurfural," *New J. Chem.*, vol. 42, pp. 18084-18095, 2018.

[13] Tan, J.-B., Wu, J.-Q., Zhao, J.-W., Xie, L.-J., and Li, G.-R., "Highly Dispersed Ultrafine Ni Particles Embedded into MOF-74 Arrays by Partial Carbonization for Highly Efficient Hydrogen Evolution," *Materials Advances*, vol. 1, pp. 1212-1219, 2020.

[14] Rovani, S., Santos, J. J., Corio, P., and Fungaro, D. A., "Highly Pure Silica Nanoparticles with High Adsorption Capacity Obtained from Sugarcane Waste Ash," *ACS Omega*, vol. 3, pp. 2618-2627, 2018.

[15] Sharma, R. K., Sharma, S., Dutta, S., Zboril, R., and Gawande, M. B., "Silica-Nanosphere-Based Organic–Inorganic Hybrid Nanomaterials: Synthesis, Functionalization and Applications in Catalysis," *Green Chemistry*, vol. 17, pp. 3207-3230, 2015.

[16] Wu, S. H., Mou, C. Y., and Lin, H. P., "Synthesis of Mesoporous Silica Nanoparticles," *Chem. Soc. Rev.*, vol. 42, pp. 3862-75, 2013.

[17] Hunge, Y. M., Yadav, A. A., Kang, S. W., Kim, H., Fujishima, A., and Terashima, C., "Nanoflakes-Like Nickel Cobaltite as Active Electrode Material for 4-Nitrophenol Reduction and Supercapacitor Applications," *J. Hazard. Mater.*, vol. 419, pp. 126453, 2021.

[18] Datta, K. J., Rathi, A. K., Kumar, P., Kaslik, J., Medrik, I., Ranc, V., Varma, R. S., Zboril, R., and Gawande, M. B., "Synthesis of Flower-Like Magnetite Nanoassembly: Application in the Efficient Reduction of Nitroarenes," *Sci Rep*, vol. 7, pp. 11585, 2017.

[19] Schummer, J., "On the Novelty of Nanotechnology: A Philosophical Essay," *In Pursuit of Nanoethics*, The International Library of Ethics, Law and Technology, 2014, pp. 15-29.

[20] Cui, C. H. and Yu, S. H., "Engineering Interface and Surface of Noble Metal Nanoparticle Nanotubes toward Enhanced Catalytic Activity for Fuel Cell Applications," *Acc. Chem. Res.*, vol. 46, pp. 1427-37, 2013.

[21] Kalra, V., Escobedo, F., and Joo, Y. L., "Effect of Shear on Nanoparticle Dispersion in Polymer Melts: A Coarse-Grained Molecular Dynamics Study," *J. Chem. Phys.*, vol. 132, pp. 024901, 2010.

[22] Padrela, L., Rodrigues, M. A., Duarte, A., Dias, A. M. A., Braga, M. E. M., and de Sousa, H. C., "Supercritical Carbon Dioxide-Based Technologies for the Production of Drug Nanoparticles/Nanocrystals - a Comprehensive Review," *Adv. Drug. Deliv. Rev.,* vol. 131, pp. 22-78, 2018.

[23] Gupta, A., Briffa, S. M., Swingler, S., Gibson, H., Kannappan, V., Adamus, G., Kowalczuk, M., Martin, C., and Radecka, I., "Synthesis of Silver Nanoparticles Using Curcumin-Cyclodextrins Loaded into Bacterial Cellulose-Based Hydrogels for Wound Dressing Applications," *Biomacromolecules,* vol. 21, pp. 1802-1811, 2020.

[24] Ma, H., Brennan, A., and Diamond, S. A., "Photocatalytic Reactive Oxygen Species Production and Phototoxicity of Titanium Dioxide Nanoparticles Are Dependent on the Solar Ultraviolet Radiation Spectrum," *Environ. Toxicol. Chem.,* vol. 31, pp. 2099-107, 2012.

[25] Pal, J., Deb, M. K., Deshmukh, D. K., and Sen, B. K., "Microwave-Assisted Synthesis of Platinum Nanoparticles and Their Catalytic Degradation of Methyl Violet in Aqueous Solution," *Appl. Nanosci.,* vol. 4, pp. 61-65, 2012.

[26] Huang, X., Li, Z., Yu, Z., Deng, X., and Xin, Y., "Recent Advances in the Synthesis, Properties, and Biological Applications of Platinum Nanoclusters," *J. Nanomater.,* vol. 2019, pp. 1-31, 2019.

[27] Zahmakiran, M. and Ozkar, S., "Metal Nanoparticles in Liquid Phase Catalysis; from Recent Advances to Future Goals," *Nanoscale,* vol. 3, pp. 3462-81, 2011.

[28] Chakraborty, I. and Pradeep, T., "Atomically Precise Clusters of Noble Metals: Emerging Link between Atoms and Nanoparticles," *Chem. Rev.,* vol. 117, pp. 8208-8271, 2017.

[29] Dreaden, E. C., Austin, L. A., Mackey, M. A., and El-Sayed, M. A., "Size Matters: Gold Nanoparticles in Targeted Cancer Drug Delivery," *Ther Deliv,* vol. 3, pp. 457-78, 2012.

[30] Majid, E., Hrapovic, S., Liu, Y., Male, K. B., and Luong, J. H., "Electrochemical Determination of Arsenite Using a Gold Nanoparticle Modified Glassy Carbon Electrode and Flow Analysis," *Anal. Chem.,* vol. 78, pp. 762-9, 2006.

[31] Polshettiwar, V. and Varma, R. S., "Green Chemistry by Nano-Catalysis," *Green Chemistry,* vol. 12, 2010.

[32] Narayanan, R. and El-Sayed, M. A., "Effect of Nanocatalysis in Colloidal Solution on the Tetrahedral and Cubic Nanoparticle Shape: Electron-Transfer Reaction Catalyzed by Platinum Nanoparticles," *J. Phys. Chem. B,* vol. 108, pp. 5726-5733, 2004.

[33] Xu, Z., He, X., Liang, M., Sun, L., Li, D., Xie, K., and Liao, L., "Catalytic Reduction of 4-Nitrophenol over Graphene Supported Cu@Ni Bimetallic Nanowires," *Mater. Chem. Phys.*, vol. 227, pp. 64-71, 2019.

[34] Kang, S., He, M., Yin, C., Xu, H., Cai, Q., Wang, Y., and Cui, L., "Graphitic Carbon Embedded with Fe/Ni Nano-Catalysts Derived from Bacterial Precursor for Efficient Toluene Cracking," *Green Chemistry,* vol. 22, pp. 1934-1943, 2020.

[35] Duan, Y., Ma, Y., Xie, Y., Li, D., Deng, D., Zhang, C., and Yang, Y., "Preparation of Pdaucu/C as a Highly Active Catalyst for the Reduction of 4-Nitrophenol by Controlling the Deposition of Noble Metals," *Chem. – An Asian J.*, vol. 16, pp. 165-173, 2020.

[36] Hofmann, S., Csanyi, G., Ferrari, A. C., Payne, M. C., and Robertson, J., "Surface Diffusion: The Low Activation Energy Path for Nanotube Growth," *Phys. Rev. Lett.*, vol. 95, pp. 036101, 2005.

[37] Sharifianjazi, F. *et al.*, "Magnetic $CoFe_2O_4$ Nanoparticles Doped with Metal Ions: A Review," *Ceram. Int.*, vol. 46, pp. 18391-18412, 2020.

[38] Kamel, S. and Khattab, T. A., "Recent Advances in Cellulose Supported Metal Nanoparticles as Green and Sustainable Catalysis for Organic Synthesis," *Cellulose,* vol. 28, pp. 4545-4574, 2021.

[39] Rathi, A. K., Gawande, M. B., Ranc, V., Pechousek, J., Petr, M., Cepe, K., Varma, R. S., and Zboril, R., "Continuous Flow Hydrogenation of Nitroarenes, Azides and Alkenes Using Maghemite–Pd Nanocomposites," *Catalysis Science & Technology,* vol. 6, pp. 152-160, 2016.

[40] Qiu, B., Xing, M., and Zhang, J., "Recent Advances in Three-Dimensional Graphene Based Materials for Catalysis Applications," *Chem. Soc. Rev.*, vol. 47, pp. 2165-2216, 2018.

[41] Campisi, S., Schiavoni, M., Chan-Thaw, C., and Villa, A., "Untangling the Role of the Capping Agent in Nanocatalysis: Recent Advances and Perspectives," *Catalysts*, vol. 6, 2016.

[42] Xu, X., Sun, L., Bai, B., Wang, H., and Suo, Y., "Interfacial Assembly of Mussel-Inspired Polydopamine@Ag Core-Shell Nanoparticles as Highly Recyclable Catalyst for Nitroaromatic Pesticides Degradation," *Sci. Total Environ.*, vol. 665, pp. 133-141, 2019.

[43] Rosbero, T. M. S. and Camacho, D. H., "Green Preparation and Characterization of Tentacle-Like Silver/Copper Nanoparticles for Catalytic Degradation of Toxic Chlorpyrifos in Water," *J.Environ. Chemical Engineer.*, vol. 5, pp. 2524-2532, 2017.

[44] Li, W., He, S.-a., Xu, W., Li, J., and Wang, X.-c., "Synthesis of BiOCl-Ag/AgBr Heterojunction and Its Photoelectrochemical and Photocatalytic Performance," *Electrochim. Acta*, vol. 283, pp. 727-736, 2018.

[45] Xiong, Z., Zhang, L. L., Ma, J., and Zhao, X. S., "Photocatalytic Degradation of Dyes over Graphene-Gold Nanocomposites under Visible Light Irradiation," *Chem Commun (Camb)*, vol. 46, pp. 6099-101, 2010.

[46] Semagina, N., Renken, A., Laub, D., and Kiwiminsker, L., "Synthesis of Monodispersed Palladium Nanoparticles to Study Structure Sensitivity of Solvent-Free Selective Hydrogenation of 2-Methyl-3-Butyn-2-Ol," *J. Catal.*, vol. 246, pp. 308-314, 2007.

[47] Guan, H., Chao, C., Lu, Y., Shang, H., Zhao, Y., Yuan, S., and Zhang, B., "PtNi Nanoparticles Embedded in Porous Silica Microspheres as Highly Active Catalysts for P-Nitrophenol Hydrogenation to P-Aminophenol," *Journal of Chemical Sciences*, vol. 128, pp. 1355-1365, 2016.

[48] Kodama, K., Nagai, T., Kuwaki, A., Jinnouchi, R., and Morimoto, Y., "Challenges in Applying Highly Active Pt-Based Nanostructured Catalysts for Oxygen Reduction Reactions to Fuel Cell Vehicles," *Nat Nanotechnol*, vol. 16, pp. 140-147, 2021.

[49] Saikia, P., Miah, A. T., and Das, P. P., "Highly Efficient Catalytic Reductive Degradation of Various Organic Dyes by Au/CeO_2 -TiO_2 Nano-Hybrid," *J. Chem. Sci.*, vol. 129, pp. 81-93, 2017.

[50] Radenahmad, N., Afif, A., Petra, P. I., Rahman, S. M. H., Eriksson, S.-G., and Azad, A. K., "Proton-Conducting Electrolytes for Direct Methanol and Direct

Urea Fuel Cells – a State-of-the-Art Review," *Renewable and Sustainable Energy Reviews,* vol. 57, pp. 1347-1358, 2016.

[51] Narayanan, R. and El-Sayed, M. A., "Catalysis with Transition Metal Nanoparticles in Colloidal Solution: Nanoparticle Shape Dependence and Stability," *J. Phys. Chem. B,* vol. 109, pp. 12663-76, 2005.

[52] Wu, S.-H. and Chen, D.-H., "Synthesis and Characterization of Nickel Nanoparticles by Hydrazine Reduction in Ethylene Glycol," *J. Colloid Interface Sci.,* vol. 259, pp. 282-286, 2003.

[53] Prasad, R., M.K, L., and Bhat, B. R., "RGO Supported Co-Ni Bimetallic Magnetically Separable Nanocatalysts for the Reduction of 4-Nitrophenol," *Synth. Met.,* vol. 219, pp. 26-32, 2016.

[54] Shah, M., Guo, Q.-X., and Fu, Y., "The Colloidal Synthesis of Unsupported Nickel-Tin Bimetallic Nanoparticles with Tunable Composition That Have High Activity for the Reduction of Nitroarenes," *Catal. Commun.,* vol. 65, pp. 85-90, 2015.

[55] Zhu, Y., Liu, Y., Gao, Y., Cheng, Q., zhao, L., and Yang, Z., "Magnetic Properties of Aristate Spherical Ni Nanoparticles Synthesized through Ultrasound Reduction Method," *Mater. Res. Bull.,* vol. 87, pp. 135-139, 2017.

[56] Li, Z., Mo, L., Kathiraser, Y., and Kawi, S., "Yolk–Satellite–Shell Structured Ni–Yolk@Ni@SiO_2 Nanocomposite: Superb Catalyst toward Methane Co2 Reforming Reaction," *ACS Catalysis,* vol. 4, pp. 1526-1536, 2014.

[57] Sharma, V. K., "Aggregation and Toxicity of Titanium Dioxide Nanoparticles in Aquatic Environment--a Review," *J Environ. Sci. Health A Tox. Hazard Subst Environ. Eng.,* vol. 44, pp. 1485-95, 2009.

[58] PILENI, M.-P., "The Role of Soft Colloidal Templates in Controlling the Size and Shape of Inorganic Nanocrystals," *Nat. mater.,* vol. 2, 2003.

[59] Zou, D., Liu, D., and Zhang, J., "From Zeolitic Imidazolate Framework-8 to Metal-Organic Frameworks (MOFs): Representative Substance for the General Study of Pioneering MOF Applications," *Energy & Environ. Mater.,* vol. 1, pp. 209-220, 2018.

[60] Jabbar, T. A. and Ammar, S. H., "Core/Shell Phosphomolybdic Acid-Supported Magnetic Silica Nanocomposite (Ni@SiO_2-PMO): Synthesis, Characterization and Its Application as a Recyclable Antibacterial Agent," *Colloid and Interface Sci. Comm.,* vol. 33, 2019.

[61] Bahuguna, A., Kumar, A., and Krishnan, V., "Carbon-Support-Based Heterogeneous Nanocatalysts: Synthesis and Applications in Organic Reactions," *Asian J.Org. Chem.*, vol. 8, pp. 1263-1305, 2019.

[62] Amrute, A. P., De Bellis, J., Felderhoff, M., and Schüth, F., "Mechanochemical Synthesis of Catalytic Materials," *Chem. – A European J.*, vol. 27, pp. 6819-6847, 2021.

[63] Dotzauer, D. M., Dai, J., Sun, L., and Bruening, M. L., "Catalytic Membranes Prepared Using Layer-by-Layer Adsorption of Polyelectrolyte/Metal Nanoparticle Films in Porous Supports," *Nano Lett.*, vol. 6, pp. 2268-72, 2006.

[64] Wang, Q.-N., Shi, L., and Lu, A.-H., "Highly Selective Copper Catalyst Supported on Mesoporous Carbon for the Dehydrogenation of Ethanol to Acetaldehyde," *ChemCatChem*, vol. 7, pp. 2846-2852, 2015.

[65] Jal, P. K., Sudarshan, M., Saha, A., Patel, S., and Mishra, B. K., "Synthesis and Characterization of Nanosilica Prepared by Precipitation Method," *Colloids and Surfaces A: Physicochemical and Engineering Aspects*, vol. 240, pp. 173-178, 2004.

[66] Sheppard, A. W., Gillespie, I., Hirsch, M., and Begley, C., "Biosecurity and Sustainability within the Growing Global Bioeconomy," *Current Opinion in Environmental Sustainability*, vol. 3, pp. 4-10, 2011.

[67] Ahmed, S., Ahmad, M., Swami, B. L., and Ikram, S., "A Review on Plants Extract Mediated Synthesis of Silver Nanoparticles for Antimicrobial Applications: A Green Expertise," *J. Adv. Res.*, vol. 7, pp. 17-28, 2016.

[68] Shekar, S., Sander, M., Riehl, R. C., Smith, A. J., Braumann, A., and Kraft, M., "Modelling the Flame Synthesis of Silica Nanoparticles from Tetraethoxysilane," *Chem. Eng. Sci.*, vol. 70, pp. 54-66, 2012.

[69] Vaibhav, V., Vijayalakshmi, U., and Roopan, S. M., "Agricultural Waste as a Source for the Production of Silica Nanoparticles," *Spectrochim. Acta A Mol. Biomol. Spectrosc.*, vol. 139, pp. 515-20, 2015.

[70] Carmona, V. B., Oliveira, R. M., Silva, W. T. L., Mattoso, L. H. C., and Marconcini, J. M., "Nanosilica from Rice Husk: Extraction and Characterization," *Industrial Crops and Products*, vol. 43, pp. 291-296, 2013.

[71] Mizutani, T., Arai, K., Miyamoto, M., and Kimura, Y., "Application of Silica-Containing Nano-Composite Emulsion to Wall Paint: A New Environmentally Safe Paint of High Performance," *Prog. Org. Coat.*, vol. 55, pp. 276-283, 2006.

[72] Lynch, B. B., Anderson, B. D., Kennedy, W. J., and Tracy, J. B., "Synthesis and Chemical Transformation of Ni Nanoparticles Embedded in Silica," *Nanoscale,* vol. 9, pp. 18959-18965, 2017.

[73] Li, P., Wei, Z., Wu, T., Peng, Q., and Li, Y., "Au−Zno Hybrid Nanopyramids and Their Photocatalytic Properties," *J. Am. Chem. Soc.,* vol. 133, pp. 5660-5663, 2011.

[74] Lu, B., Zhang, Z., Hao, J., and Tang, J., "Facile Synthesis of Au@ Fe_3O_4–Graphene and Pt@Fe_3O_4–Graphene Ternary Hybrid Nanomaterials and Their Catalytic Properties," *RSC Adv.,* vol. 4, 2014.

[75] Xia, Y. S. a. Y., "Shape-Controlled Synthesis of Gold and Silver Nanoparticles," *SCIENCE,* vol. 298, pp. 2176-2178, 2002.

[76] Tang, J., Huang, J., and Man, S. Q., "Preparation of Gold Nanoparticles by Surfactant-Promoted Reductive Reaction without Extra Reducing Agent," *Spectrochim. Acta A Mol. Biomol. Spectrosc.,* vol. 103, pp. 349-55, 2013.

[77] Abduraimova, A., Molkenova, A., Duisembekova, A., Mulikova, T., Kanayeva, D., and Atabaev, T. S., "Cetyltrimethylammonium Bromide (CTAB)-Loaded SiO_2-Ag Mesoporous Nanocomposite as an Efficient Antibacterial Agent," *Nanomaterials (Basel),* vol. 11, 2021.

[78] Yusoff, A. H. M., Salimi, M. N., and Jamlos, M. F., "Synthesis and Characterization of Biocompatible Fe_3O_4 Nanoparticles at Different Phase," 2017.

[79] Titus, D., James Jebaseelan Samuel, E., and Roopan, S. M., "Chapter 12 - Nanoparticle Characterization Techniques," in *Green Synthesis, Characterization and Applications of Nanoparticles*, Shukla, A. K. and Iravani, S., Eds.: Elsevier, 2019, pp. 303-319.

[80] Garino, N. *et al.*, "Microwave-Assisted Synthesis of Reduced Graphene Oxide/SnO_2 Nanocomposite for Oxygen Reduction Reaction in Microbial Fuel Cells," *ACS Appl. Mater. Interfaces,* vol. 8, pp. 4633-43, 2016.

[81] Rashed, A. E. and El-Moneim, A. A., "Two Steps Synthesis Approach of MnO_2/Graphene Nanoplates/Graphite Composite Electrode for Supercapacitor Application," *Materials Today Energy,* vol. 3, pp. 24-31, 2017.

[82] Ameh, E. S., "A Review of Basic Crystallography and X-Ray Diffraction Applications," *Inter. J. Adv. Manufact. Techn.,* vol. 105, pp. 3289-3302, 2019.

[83] Bharath, G., Alhseinat, E., Ponpandian, N., Khan, M. A., Siddiqui, M. R., Ahmed, F., and Alsharaeh, E. H., "Development of Adsorption and Electrosorption Techniques for Removal of Organic and Inorganic Pollutants from Wastewater Using Novel Magnetite/Porous Graphene-Based Nanocomposites," *Sep. Purif. Technol.*, vol. 188, pp. 206-218, 2017.

[84] Ul-Hamid, A., *A Beginners' Guide to Scanning Electron Microscopy*. Switzerland: Springer Nature, 2018.

[85] Semnani, D., "7 - Geometrical Characterization of Electrospun Nanofibers," in *Electrospun Nanofibers*, Afshari, M., Ed.: Woodhead Publishing, 2017, pp. 151-180.

[86] Gholampour, A., Valizadeh Kiamahalleh, M., Tran, D. N. H., Ozbakkaloglu, T., and Losic, D., "From Graphene Oxide to Reduced Graphene Oxide: Impact on the Physiochemical and Mechanical Properties of Graphene-Cement Composites," *ACS Appl. Mater. Interfaces.*, vol. 9, pp. 43275-43286, 2017.

[87] Colpan, C. O., Nalbant, Y., and Ercelik, M., "4.28 Fundamentals of Fuel Cell Technologies," in *Comprehensive Energy Systems*, Dincer, I., Ed. Oxford: Elsevier, 2018, pp. 1107-1130.

[88] Ebnesajjad, S., "Surface and Material Characterization Techniques," in *Handbook of Adhesives and Surface Preparation*, Ebnesajjad, S., Ed. Oxford: William Andrew Publishing, 2011, pp. 31-48.

Chapter-2

Experimental

2.1 Materials and Chemicals

The starting materials, nickel chloride hexahydrate ($NiCl_2.6H_2O$), sodium hydroxide (NaOH), sodium borohydride ($NaBH_4$), sulfuric acid (H_2SO_4, 98%), 4-nitrophenol (4-NP), were purchased from Sigma-Aldrich, Germany. Hydrazine hydrate (H_6N_2O 80%), hydrochloric acid (HCl, 37%), ethanol (C_2H_5OH) were obtained from Lab-Scan, Ireland and ethylene glycol, Cetyltrimethylammonium Bromide (CTAB), butyl alcohol ($C_4H_{10}O$) were purchased from Merck Specialties Private Limited, India. All aqueous solutions were prepared using deionized water obtained from a Nano-pure water system (Barnstead Nano-pure, Thermo Scientific, USA). Sonication was performed using a digital ultrasonic bath (Powersonic 505, Hwashin, S. Korea). The reagents and solvents were used without further purification.

2.2 Materials Characterizations

The crystalline structures of the capped SiO_2 NPs, Ni NPs and Ni-SiO_2 nano-catalysts were obtained by the X-ray diffraction (XRD) method on a RigakuD/max-TTR-III diffractometer using Kβ filter 1D for Cu radiation with a scan range of 10−80° (2θ) at a rate of 5°/min. The morphology and the sizes of the samples were studied by Field Emission Scanning Electron Microscopy (FESEM) using JSM-7600F, Tokyo, Japan. The chemical composition (atomic per cent) of the samples was determined by energy-dispersive X-ray (EDX) spectrometry (Hitachi S-4800 Japan). Fourier-transform infrared (FTIR) spectra of the prepared nanocomposites were recorded on a SHIMADZU FT-IR-8400 spectrophotometers from 4000 to 400 cm^{-1} (with a 2 cm^{-1} resolution and 60 times scanning) based on the KBr method. UV−vis spectroscopy was performed on a UV1800PC produced by Shanghai AuCy Scientific Instrument Co., Ltd, China.

2.3 Preparation of Sodium Silicate

The synthesis of SiO_2 NPs was carried out from sugarcane bagasse with various modifications according to the reported methods [1]. SCB was collected from a sugarcane juice store in Dhaka. The collected bagasse was cut into pieces and rinsed with tap water repeatedly until the waste was clear. It was oven-dried at 120 °C overnight. The SCB was then burned in the open air and placed in a muffle furnace for 5 hours to pyrolysis at 700 °C until it reached a constant weight.

The appearance of the white-gray color of the sugarcane bagasse ash (SCBA) confirmed that a large amount of carbon atoms was disappeared. SCBA was treated using 50 mL of 0.1 mol L^{-1} HCl (37 wt.%), stirred for 2 hours at room temperature, and then stored overnight. The suspension was filtered using filter paper, and the solid residue was washed with deionized water to remove metallic ions. Afterward, the solid was dried in the oven at 120 °C for overnight before further use. About 1 g of washed SCBA was mixed with 1.5 g of solid NaOH (ratio of 1:1.5, w/w) to obtain a homogeneous mixture, and the mixture was heated for 1 hour in a muffle furnace at 400 °C. At the end of the treatment, the resulting fused mixture was dissolved in 100 mL of deionized water and refluxed for 4 hours. To reduce solid residue, the obtained mixture was filtered using a Whatman No 41. The sodium silicate (Na_2SiO_3) formed as the following reaction, remaining in the filtrate solution, will be employed as a silica precursor or source [2-4].

2.4 Preparation of Capped SiO_2 Nanoparticles

In a 500 mL round bottom flask, 100 mL water and 100 mL butyl alcohol (1:1, v/v) were poured. Next, 4.5 g of CTAB was added as a capping agent into the microemulsion solution and stirred at room temperature until the capping agent was dissolved. Then 40 mL of sodium silicate solution was added to this mixture in the round bottle flask. Finally, 0.5 mol L^{-1} sulfuric acid solution was added dropwise to this solution until the pH decreased to 4, and the resultant gel was refluxed at 60 °C for 8 hours under stirring. The resulting capped SiO_2 NPs were separated by centrifugation and washed with deionized water several times until its pH reached 7,

then dried in a vacuum oven at 120 °C. Thus obtained SiO_2 NPs were collected in a vial and kept in a vacuum desiccator.

2.5 Preparation of Ni Nanoparticles

The nickel nanoparticles were prepared through reducing nickel chloride hexahydrate ($NiCl_2.6H_2O$) by hydrazine hydrate (80 wt.%) according to modified Wu's method [5]. Typically, 0.5 g of $NiCl_2.6H_2O$ was dissolved directly in 20 mL of ethylene glycol in a 250 mL round bottom flask. This step was followed by adding 3.33 ml of hydrazine hydrate by stirring, which acts as a reducing agent, and the color was turned into light green to pale violet. Then, a solution of sodium hydroxide (0.43 g) dissolved in 5 mL ethylene glycol was added to the mixture and stirred at 80 °C for 1 hour. As a result, the color of the solution was gradually changed to black. After adding the reducing agent and sodium hydroxide, the pH was raised to 12. The resulting Ni NPs was thoroughly washed in ethanol and dried for 24 hours under vacuum at 60 °C.

2.6 Preparation of Capped Ni-SiO_2 Nano-catalyst

A single-step, chemical reduction approach was used to synthesize the capped Ni-SiO_2 nano-catalysts. To synthesize the capped Ni-SiO_2 nano-catalyst, (with Ni and SiO_2 mass ratio of 1:2) 300 mg of SiO_2 NPs was mixed with 30 mL ethylene glycol in a 250 mL round bottom flask and ultrasonicated for 1 hour. Then, 608 mg of $NiCl_2.6H_2O$ was dissolved in SiO_2 NPs suspension followed by sonication for 15 min. Next, 3.4 mL of reducing agent hydrazine hydrate (80 wt%) was added to the flask with vigorous stirring and the color of the solution was immediately changed from light green to pale violet. Subsequently, a specified amount of 0.486 g of NaOH was added until the pH reached to 12 and the mixture was heated at 80 °C for 1 hour under N_2 atmosphere. The synthesized black fluffy solid products of capped Ni-SiO_2 (1:2) nano-catalyst was collected by an external magnet, washed with deionized water and absolute ethanol several times, then dried in a vacuum oven at 60 ^oC for 24 hours. The same method was used to prepare a series of capped Ni-SiO_2 nano-catalysts with the same theoretical loading, and different mass ratios of Ni and SiO_2 (1: 1 and 1: 3) were also prepared.

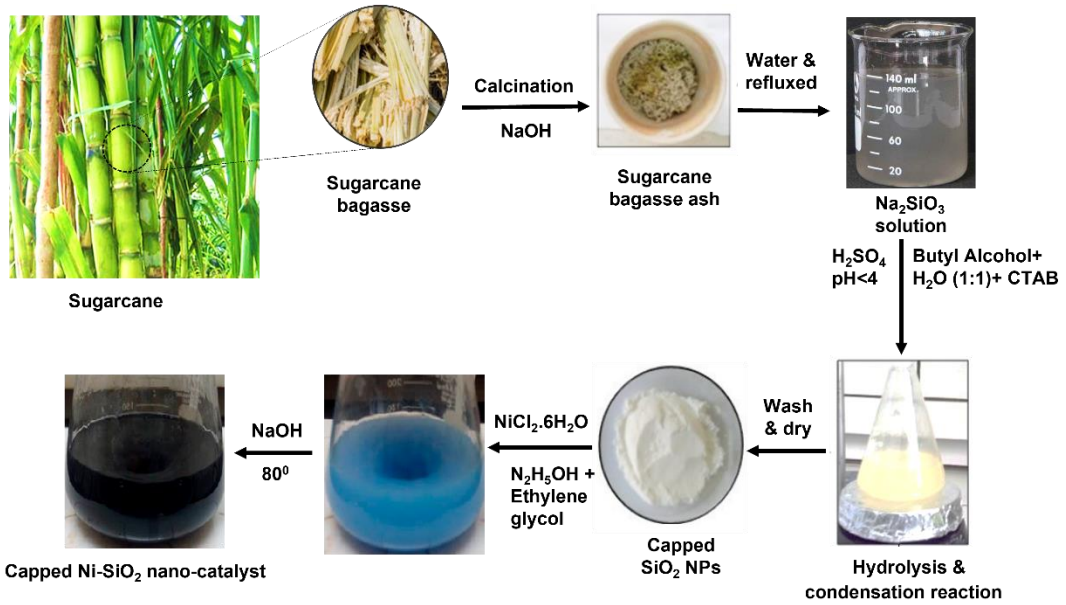

Scheme 2.1: A schematic illustration of the preparation of capped Ni-SiO_2 nano-catalyst from sugarcane bagasse through thermo-chemical methods.

2.7 Catalytic Reduction

The catalytic activity of the capped SiO_2 NPs, Ni NPs and capped Ni-SiO_2 nano-catalyst was investigated employing the reduction of 4-NP by $NaBH_4$, which was chosen as a model reaction. In a typical procedure, 200 µL of 4-NP solution (1 mM, 25mL) was added to 5 mL of deionized water in a vial. A small amount of solution from the vial was taken in a quartz cuvette, and the absorbance at 317 nm was monitored on a UV-Vis spectrophotometer in the wavelengths ranging from 250 to 500 nm at room temperature. Then, 1 mL of freshly prepared $NaBH_4$ (0.2 M, 25mL) aqueous solution, 200 µL of 4-NP (1 mM) solution, and 5 mL of deionized water were added into a 25 mL vial with stirring. Due to the reducing agent of $NaBH_4$ aqueous solution, the solution was immediately turned from pale yellow to bright yellow. As in the previous method, a small amount of the mixed solution was placed in a quartz cuvette to measure the changes in absorbance at 400nm at various time intervals without catalyst. Finally, 2 mg of capped Ni-SiO_2 (mass ratio 1:2) nano-catalyst was added to the prepared solution of $NaBH_4$ and 4-NP in the vial to initiate the

reduction reaction. The progress of the reaction was monitored using UV−vis absorption spectroscopy and recorded immediately at a regular interval of 2 min. The sampling procedure was continued until the color of the mixture changed from bright yellow to colorless, and absorbance turned into zero, indicating that the catalysis was completed. The same performance was repeated for capped SiO_2 NPs, Ni NPs, and different mass ratios (1:1, 1:3) of capped Ni-SiO_2 nano-catalysts at various amounts (1- 4 mg) for the reduction of 4-NP using $NaBH_4$ solution.

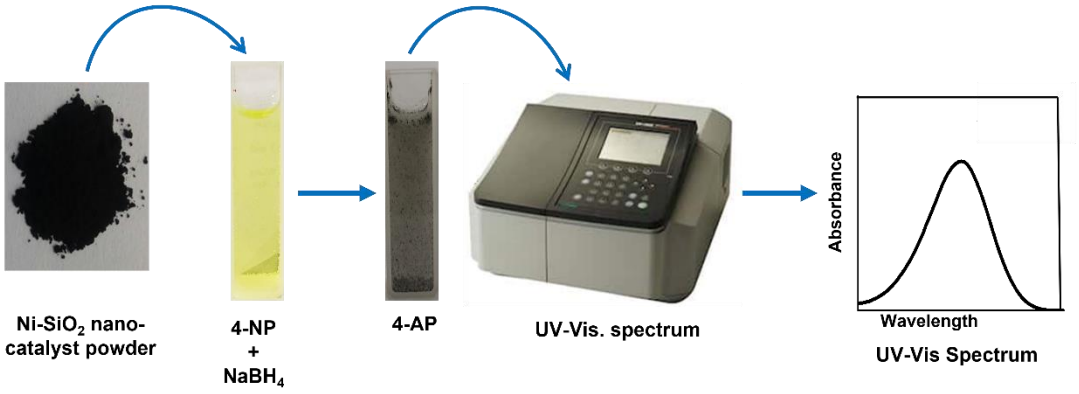

Scheme 2.2: Schematic steps in the reduction of the 4-NP to 4-AP with capped Ni-SiO_2 nano-catalyst employing UV−Vis absorption spectroscopy.

2.8 References

[1] Suzimara, R., Jonnatan, J. S., Paola, C, and Denise, A. F., "Highly Pure Silica Nanoparticles with High Adsorption Capacity Obtained from Sugarcane Waste Ash," *J Am Chem Soc,* vol. 3, pp. 2618−2627, 2018.

[2] Rodrigo, H. A., Thais, V. da S. R., Suzimara, R., and Denise, A. F., "Green Synthesis and Characterization of Biosilica Produced from Sugarcane Waste Ash," *J. Chem.*, pp 9, 2017.

[3] Xiaozhong, W., Wenhuai, L., Guangshan, Z., Shilun, Q., Dongyuan, Z., and Bing, Z., "Effects of ammonia/silica molar ratio on the synthesis and structure of bimodal mesopore silica xerogel," *MICROP M M*, vol. 71, pp. 87–97, 2004.

[4] Hassan, A. F., Abdelghny, A. M., Elhadidy, H., and Youssef, A. M., "Synthesis and characterization of high surface area nanosilica from rice husk ash by surfactant-free sol–gel method," *J Sol-Gel Sci Technol*, vol. 69, pp 465–472, 2014.

[5] Szu-Han, W., and Dong-Hwang C., "Synthesis and characterization of nickel nanoparticles by hydrazine reduction in ethylene glycol," *J. Colloid Interface Sci*, vol. 259, pp 282–286, 2003.

Chapter-3

Results and Discussion

3.1 Synthesis of Nano-catalysts

A schematic illustration of the fabrication of well-dispersed Ni NPs on SiO_2 nano surface through a capping agent is shown in Scheme 3.1. The SiO_2 NPs was synthesized from SCBA. SCBA was produced by burning sugarcane bagasse which contains various impurities, particularly different salts (Al_2O_3, Fe_2O_3, TiO_2 etc.) and carbon contents [1]. The primary element of SCBA is SiO_2, which is 81.60 wt%, indicating that this material is suitable to use as a source of silica through producing sodium silicate solution [2, 3]. The pretreatment method was carried out to wash away excess salts, organic compounds, and low-solubility components [3]. Sodium silicate (Na_2SiO_3) solution was separated from SCBA by reacting with sodium hydroxide pellet at 400 °C [4]. Sodium hydroxide was melted at 400 °C, which increased silicon extraction and purity. The charge density of negatively charged silica species (*i.e.*, silicates) increases along with the pH under alkaline circumstances (pH > 7.0), which can only associate with the cationic Na^+ ion through strong electrostatic contact [5]. The production of SiO_2 NPs from sodium silicate solution is based on hydrolysis (production of silanol groups) and condensation (siloxane formation) reaction with sulfuric acid in a biphasic medium in the presence of CTAB [5, 6]. CTAB acts as micellar medium and assists in controlling nanoparticle size to prevent the self-aggregation of nanoparticles by capping the surface charge. It is a crucial stabilizer for modification and formation of surface recombination centers, which can disperse metal nanoparticles significantly [7-10]. The reaction was completed under an emulsion/biphasic medium by utilizing butanol to form an isotropic liquid mixture of water, oil and surfactant, as first reported by Hoar *et al.* [11]. Surfactant molecules orient themselves to form spherical aggregates in the continuous phase of water-in-oil (w/o) microemulsions, which are commonly utilized to produce silica NPs. In this approach, the co-condensation method using sulfuric acid generates a white solid with low dispersion in both media, easily removed by centrifugation. In acidic solutions, the silicate ions react with hydrogen ions to form silicic acids, which decompose into hydrated silicon dioxide gel. The prepared SiO_2 NPs was 99.08 ± 0.99 wt.% pure observed in Energy Dispersive X-ray (EDX) analyses, as shown in Figure 3.7.

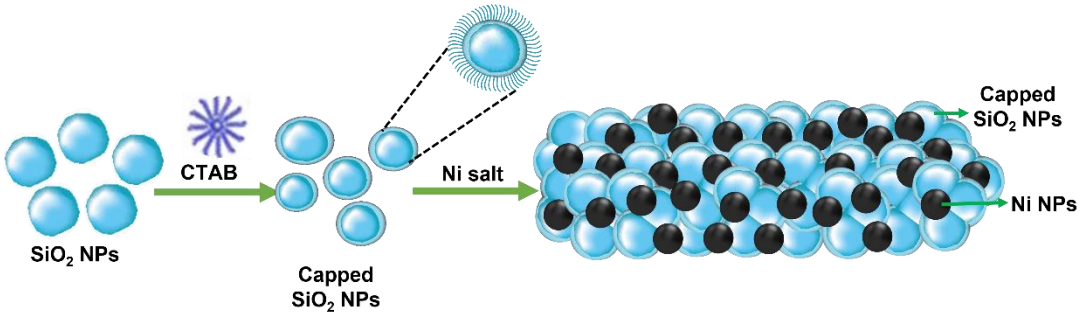

Scheme 3.1: Schematic illustration for the fabrication of capped Ni-SiO_2 nano-catalyst.

To prepare capped Ni-SiO_2 nano-catalyst, the SiO_2 NPs was mixed with ethylene glycol solution of $NiCl_2.6H_2O$ with the reducing agent hydrazine hydrate (80% $N_2H_4.H_2O$) in the presence of sodium hydroxide. By pouring 80% $N_2H_4.H_2O$ solution into a $NiCl_2$ aqueous solution, a Ni complex ($Ni[(N_2H_4)_3]Cl_2$) between $NiCl_2$ and N_2H_4 (pale violet precipitate) was actively formed showed in Eq-1 [12].

$$NiCl_2 + 3N_2H_4 \rightarrow Ni[(N_2H_4)_3]Cl_2 \quad [1]$$

$Ni[(N_2H_4)_3]Cl_2$ is less stable and may decompose into $Ni[(N_2H_4)_2]Cl_2$ with the release of N_2H_4. The $[Ni(NH_3)_6]Cl_2$ was reported to appear when $[Ni(N_2H_4)_2]Cl_2$ is heated to a high temperature. (Eq-2 and 3)

$$Ni[(N_2H_4)_3]Cl_2 \rightarrow [Ni(N_2H_4)_2]Cl_2 + N_2H_4 \quad [2]$$

$$[Ni(N_2H_4)_2]Cl_2 + 5/2\ N_2H_4 \rightarrow [Ni(NH_3)_6]Cl_2 + 3/2N_2\ (g)\uparrow \quad [3]$$

The decomposition of a Ni complex in a highly alkalic environment (pH ~ 11) would result in the formation of $Ni(OH)_2$, and it can be reduced by N_2H_4 from the following reaction [13-15].

$$2Ni^{2+} + N_2H_4 + 4OH^- \rightarrow 2Ni + N_2 + 4H_2O \quad [4]$$

Finally, the capped Ni-SiO_2 nano-catalyst was obtained through an *in-situ* decomposition and reduction procedure at high temperatures in a hydrogen atmosphere.

3.2 Functional Group Identification by FTIR

Fourier Transform Infrared Spectroscopy (FTIR) was used to analyze the functional groups of the prepared nano-catalysts, as shown in Figure 3.1(a-d). The presence of IR absorbance bands at 800, 1059, 1641 and 3,452 cm^{-1} has confirmed the formation of

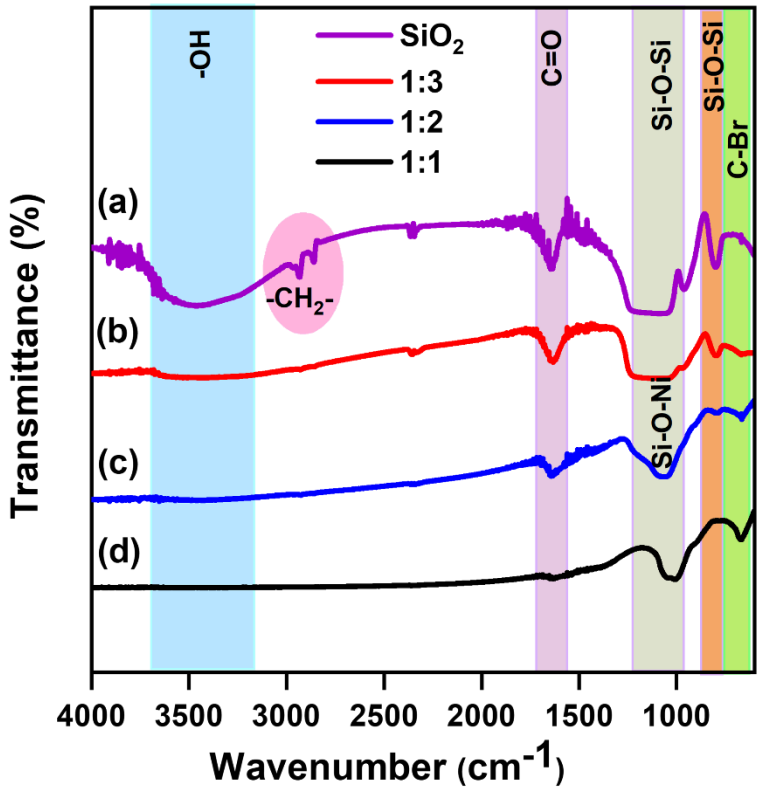

Figure 3.1: FTIR spectra of (a) capped SiO_2 NPs, capped Ni-SiO_2 nano-catalyst at the mass ratios of (b) 1:3, (c) 1:2 and (d) 1:1.

silica [16, 17]. Hence, Figure 3.2 (a) depicts the two separate symmetric and asymmetric stretching bands of CH_2 at 2933 and 2862 cm^{-1}, respectively which is associated with the presence of CTAB [18]. The C-Br stretching frequency of the CTAB appears at 621 cm^{-1} [19]. However, as shown in Figure 3.2 (b-d) from the expanded FTIR spectra, it is indicated that as compared to capped SiO_2 NPs, all the SiO_2-supported nano-catalysts bands are slightly moved, which can be attributed to the metal loading [20]. The very strong band at 1060 cm^{-1} indicated the Si-O-Ni band, which proved the formation of capped Ni-SiO_2 nano-catalyst. In addition, there is a significant change in Ni-SiO_2 nano-catalysts with a mass ratio of 1:2 and 1:1 in the

FTIR spectra. These results indicate that decreasing of SiO_2 NPs in the catalyst changes the absorption spectra.

Table 3.1: FTIR Characteristic peak and corresponding interpretations for SiO_2 NPs.

Wave number (cm^{-1})	Interpretations
3,452	–OH stretching
2933	CH_2 symmetric stretching
2862	CH_2 asymmetric stretching
1641	C=C stretching
1060	Si-O-Ni asymmetric stretching
954	–CH vibration
800	Si-O-Si symmetric stretching
621	C-Br stretching

3.3 Structural Analysis by XRD

X-ray Diffraction **(**XRD) patterns of the synthesized capped SiO_2 NPs, Ni NPs and capped Ni-SiO_2 nano-catalysts were performed for purity and crystallinity of structural analysis, as shown in Figure 3.2. Broad diffraction peak at 2θ value of 22.42º (101) for SiO_2 NPs indicates formation of amorphous silica by the low-temperature vapor-phase hydrolysis process [21- 23]. The characteristic three peaks for Ni NPs are found at 2θ = 44.62º, 51.87º and 76.44º, which corresponded with the (111), (200) and (220) planes of pure face centered cubic (fcc) structure Ni, respectively, according to a standard PDF card (JCPDS No. 04-0850) [2].

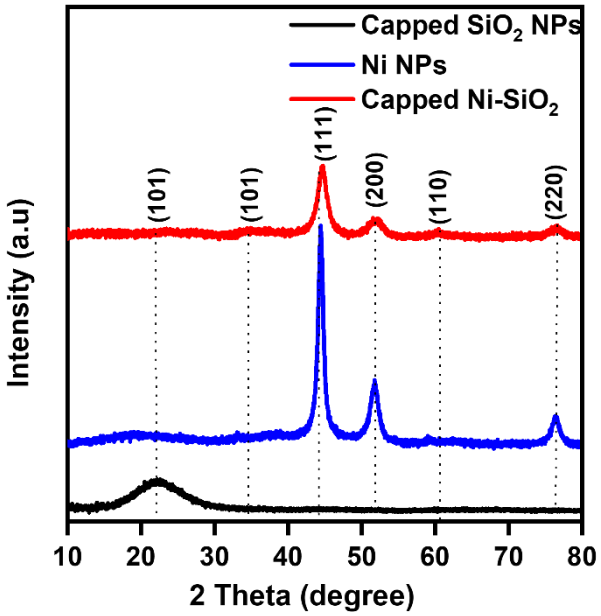

Figure 3.2: XRD spectra of capped SiO_2 NPs, Ni NPs and capped Ni-SiO_2 (1:2) nano-catalysts.

For the capped Ni-SiO_2 nano-catalyst, there are three diffraction peaks detected at around 44.62°, 51.87° and 76.44°, respectively, which are attributed to the (111), (200) and (220) crystal planes of the fcc structure of Ni NPs (JCPDS No. 04-0850), respectively. Sharp peak at 2θ of 44.62° is indicated the formation Ni-SiO_2 nano-catalyst. The XRD diffraction peaks intensity indicates the higher crystallinity of Ni-SiO_2 nano-catalyst than SiO_2 NPs. The characteristic diffraction peaks of 2θ value of 35.5° (101) and 60° (110) indicate that a small amount of $Ni(OH)_2$ is formed in the nano-catalyst, which is negligible [24, 25].

3.4 Surface Morphology Study by FESEM

Field emission scanning electron microscope (FESEM) was used to analyze the morphology and surface microstructure of prepared capped SiO_2 NPs, Ni NPs and capped Ni-SiO_2 nano-catalysts. Figure 3.3(a) depicts the morphology of the capped SiO_2 NPs synthesized from sugarcane bagasse. It can be seen that spherical SiO_2 with different size were obtained. The thin film structure on SiO_2 NPs with the Presence of scattered pores and soft spongy in SiO_2 NPs indicates the capping of CTAB. The size variation, related to emission of organic materials during the bagasse hardened, between 5 and 500 μm. The microspheres with porous structures are useful for loading Ni NPs with variety of size by embedding them among the nanoparticles.

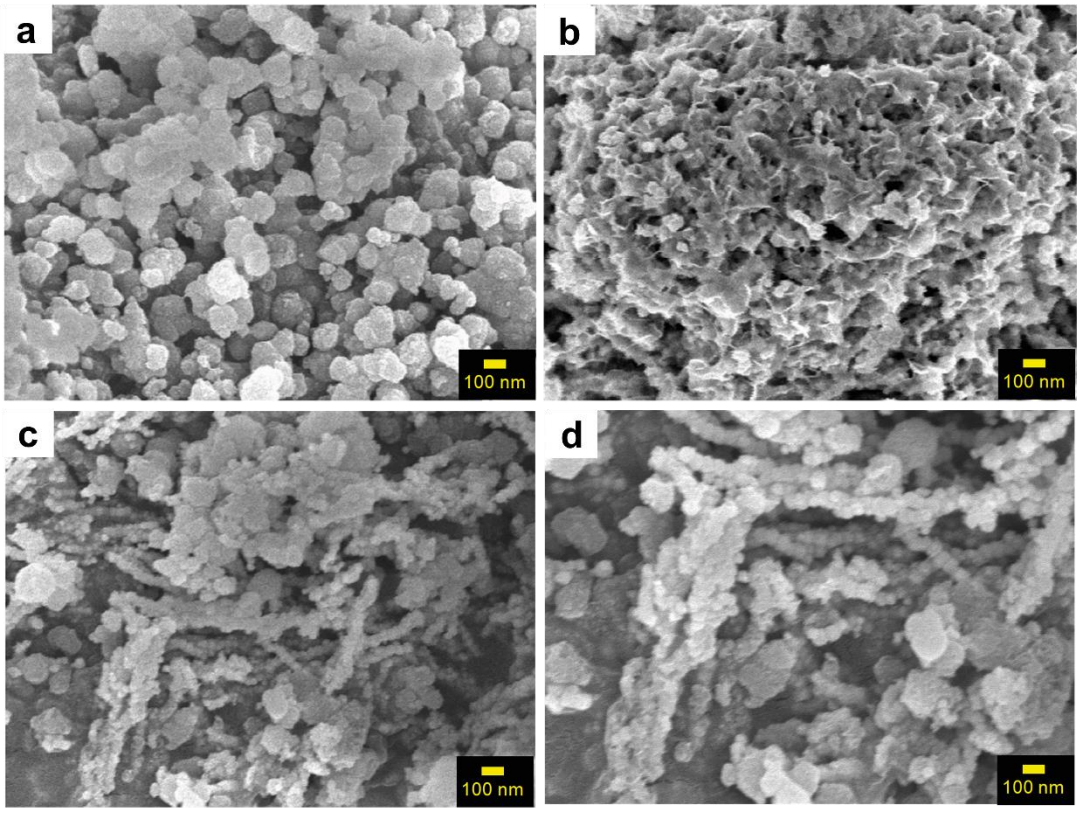

Figure 3.3: FESEM images for the surface of (b) capped SiO_2 NPs, (b) Ni NPs, and (c, d) capped Ni-SiO_2 nano-catalyst.

Figure 3.3 (b) shows the FESEM of Ni NPs are Spherical particles with coral cluster. From Figure 3.4 (b), it can be seen that strong aggregation and staking of Ni NPs with different morphologies and diameters which responsible to from metal clusters. These kinds of structure render the performance of Ni NPs.

Figure 3.3(c, d) illustrates the FESEM of capped Ni-SiO_2 nano-catalyst. The loading of Ni NPs had little effect on the morphology of the SiO_2 surface, shown in Figure 3.3(c-d), demonstrating that the Ni NPs were successfully loaded onto the surface of the SiO_2 NPs with the help of capping agent CTAB. On the surface of SiO_2 NPs, the loaded Ni NPs are uniformly dispersed [26]. The Ni NPs forms a well-dispersed nano-chain with SiO_2 NPs. The size of Ni NPs is larger than the pore size of SiO_2, but due to strong interfacial interaction with the capping agent, Ni NPs can be easily immobilized on the SiO_2 surface. It can be seen that the aggregation of Ni NPs was controlled using capped SiO_2 NPs. The loaded Ni NPs increase the stability of nano-catalysts while also providing many active sites for catalytic reduction of nitroaromatic compounds. More characterization of the elemental composition (atomic percent) of the as-synthesized Ni-SiO_2 nano-catalyst is investigated using energy-dispersive X-ray (EDX) spectrometry, as shown in the Figure 3.7. The EDX spectrum of nano-catalyst confirm that the elements of Ni NPs are existed and are nicely dispersed on the SiO_2 nano matrix shows in Figures 3.3(c, d).

3.5 Size Distribution Study by FESEM

The size distribution of prepared materials is measured by ImageJ software and displayed in Figures 3.4, 3.5 and 3.6 of capped SiO_2 NPs, Ni NPs and capped Ni-SiO_2 nano-catalyst, respectively. In that software firstly required SEM image was inserted, and the size was plotted against the total number present in percentage (frequency %). Figure 3.4(b) depicts the average particle size of SiO_2 NPs calculated from the Figure 3.4(a) using ImageJ software processing. The size range of SiO_2 NPs is distributed throughout the surface, the minimum particle size is 30 nm, and the maximum size is 88 nm. The average diameter of the particle is 64 nm.

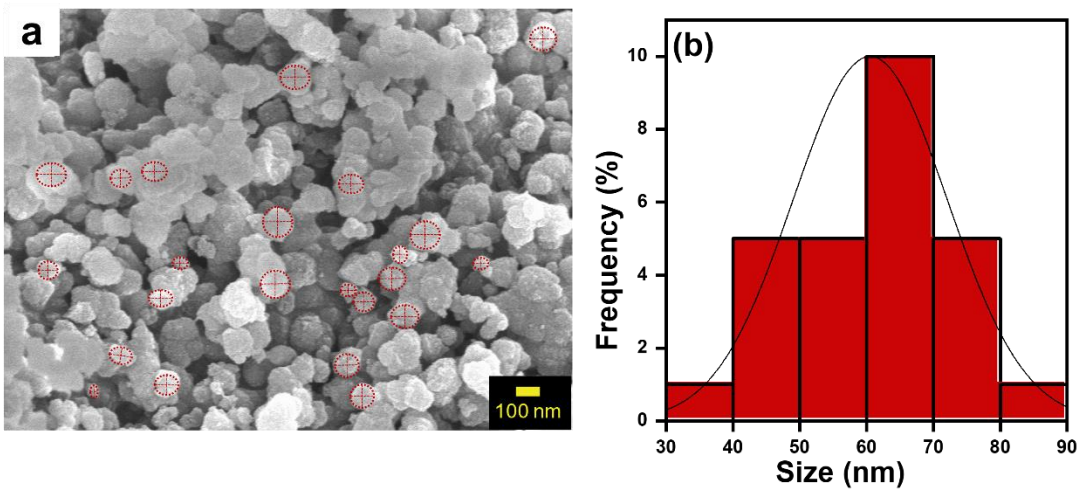

Figure 3.4: (a) FESEM image and (b) size distribution (equivalent diameter) histograms of capped SiO_2 NPs. .

Figure 3.5(b) shows Ni particles range from 25-74 nm are distributed throughout the surface, and the average size of Ni NPs of 48 nm which was calculated from the FESEM of Figure 3.5(a) using ImageJ software processing system.

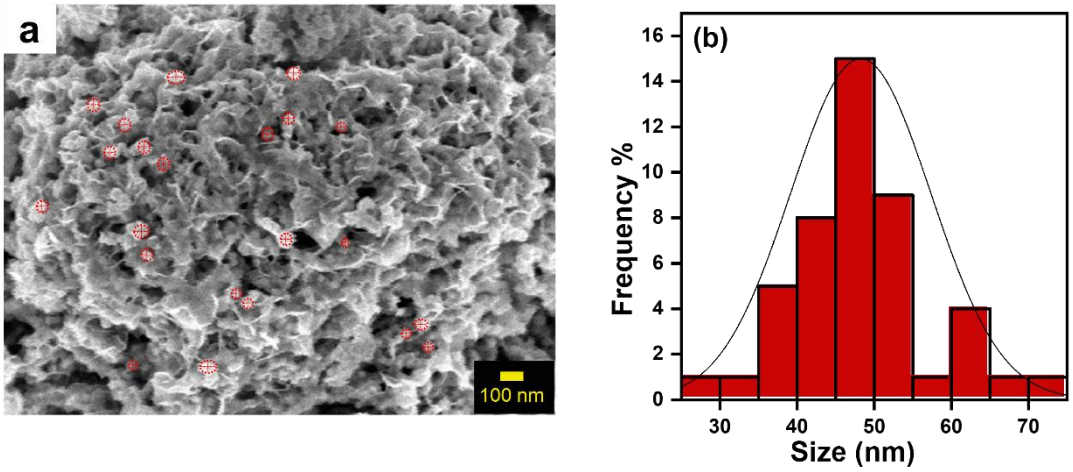

Figure 3.5: (a) FESEM image and (b) size distribution (equivalent diameter) histograms of Ni NPs.

The surface morphology of capped Ni-SiO_2 nano-catalyst in Figure 3.6(b). shows that the average diameter of the composites is 54 nm and ranges from 35-78 nm are distributed throughout the surface of the capped Ni-SiO_2 nano-catalyst shows in Figure 3.6(a).

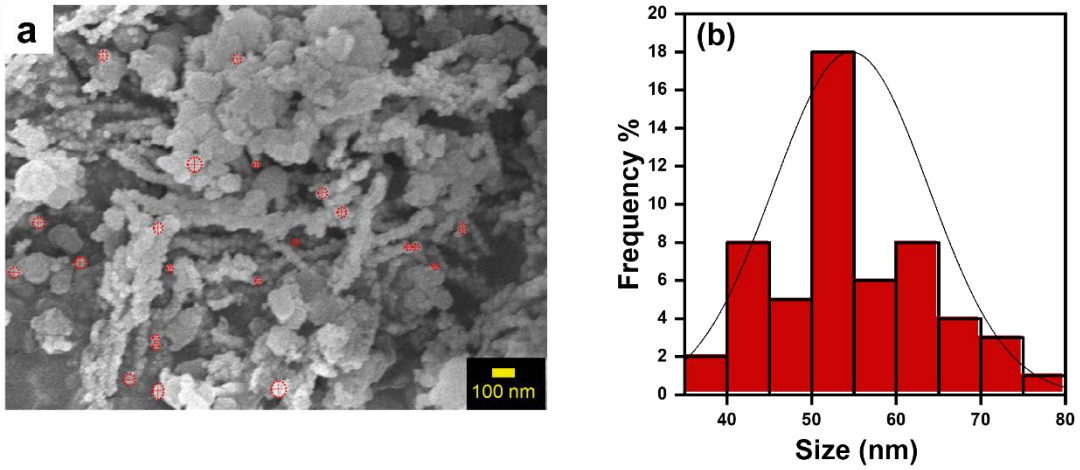

Figure 3.6: (a) FESEM image and (b) size distribution (equivalent diameter) histograms of Ni NPs of capped Ni-SiO_2 nano-catalyst.

3.6 Chemical Composition Study Using EDX Spectroscopy

The Energy Dispersive X-ray (EDX) spectrum was performed to determine the elemental composition of prepared capped SiO_2 NPs, Ni NPs, and capped Ni-SiO_2 nano-catalyst, as shown in Figure 3.7(a-c). In Figure 3.7(a) for SiO_2 NPs, the peaks observed at 0.525 keV and 1.739 keV correspond to the K shell of Si and O, respectively. Figure 3.7(b) exhibits that the peaks appear at 0.851 keV for the L shell of Ni. Figure 3.7(c) indicates the peaks at 0.525 and 0.1.739 and 0.851 keV of O, Si to K shell and Ni to L shell, respectively. All the atoms and their percentages are summarized in Table 3.2.

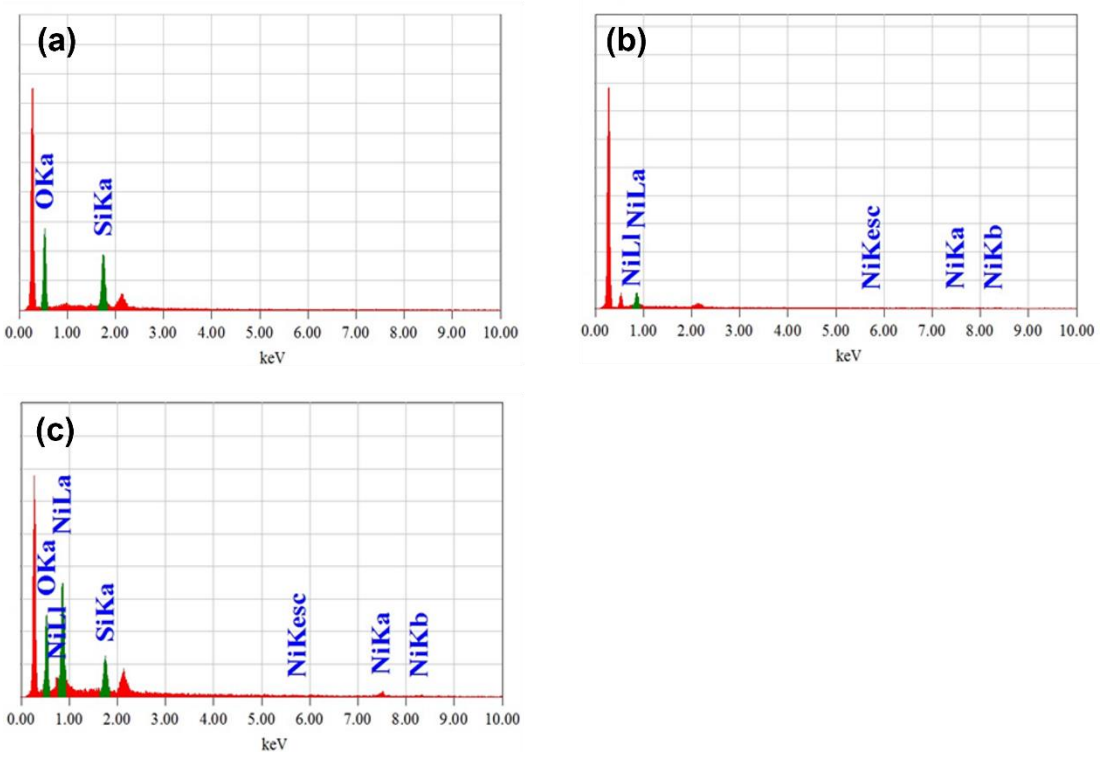

Figure 3.7: EDX spectra of (a) capped SiO_2 NPs, (b) Ni NPs, and (c) capped Ni-SiO_2 nano-catalyst.

Table 3.2: Elemental composition of Ni NPs, SiO_2 NPs, and capped Ni-SiO_2 nano-catalyst

Samples	The atomic percentage of elements in the samples		
	Ni	Si	O
Ni	99.34		
SiO_2		21.23	78.77
Capped Ni-SiO_2 (1:2)	38.58	10.33	51.09

3.7 Catalytical Reduction of 4-Nitrophenol

3.7.1 Reduction of 4-Nitrophenol by $NaBH_4$

Catalytic reduction of 4-NP to 4-AP in the presence of $NaBH_4$ is a common method for evaluating catalytic performance where 4-NP corresponds a model reaction. The reaction process is monitored by an UV–vis spectrometer. Under a neutral or acidic condition without $NaBH_4$, the 4-NP solution exhibits a strong absorption peak at 317 nm, monitored through UV−visible absorption spectroscopy as can be seem in Figure 3.8(a) [27]. Figure 3.8(b) shows the UV-vis spectra of 4-NP aqueous solution (0.035 mM) reduced by $NaBH_4$ (35 mM).

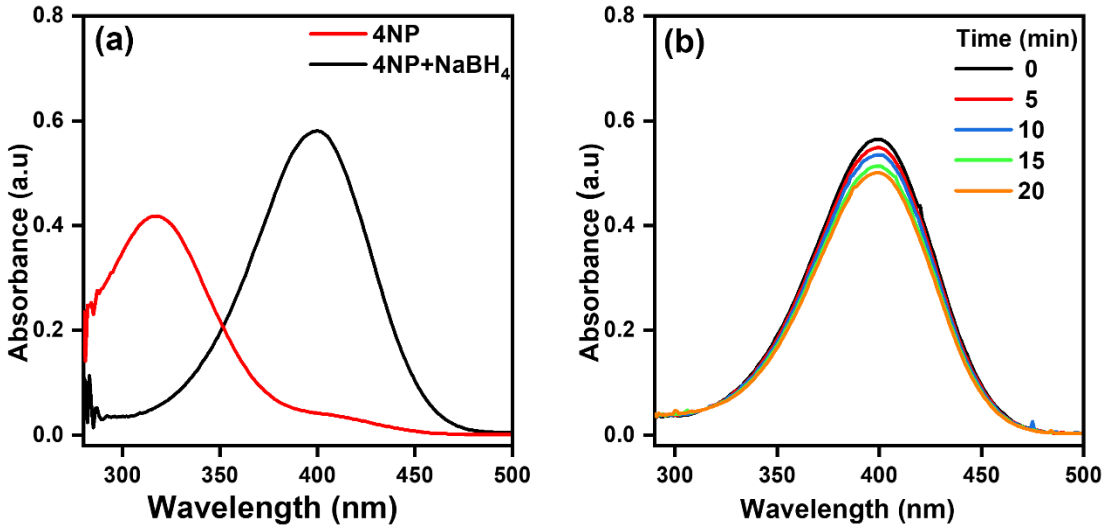

Figure 3.8: (a) Comparative UV-vis absorption spectral changes of 4-NP without $NaBH_4$, and 4-nitrophenolate ion generated by addition of $NaBH_4$. (b) Time dependent UV–Vis spectra for the reduction of 4-NP using $NaBH_4$ but without catalyst.

Upon the addition of freshly prepared $NaBH_4$, 4-NP converts it into a 4-nitrophenolate ion with an absorption peak at 400 nm shows in Figure 3.8(a) [27, 28]. The light-yellow color changes into a bright yellow color because of the change in alkalinity of the mixture, thus resulting in the formation of a 4- nitrophenolate ion. The spectrum reveals that a minor quantity of 4-NP was reduced, indicating that the reaction rate is very slow and will take a long time to complete the reaction.

3.7.2 Reduction of 4-Nitrophenol by Capped SiO_2 NPs

Catalytic performance of capped SiO_2 estimated utilizing the 4-NP solution NPs is shown in Figure 3.9. It was found that no significant reduction reaction occurs in the presence of capped SiO_2 NPs, even after 24 h of investigation, demonstrating that capped SiO_2 NPs cannot be used as the catalyst for the reduction of 4-NP, and this reduction reaction cannot continue without a catalyst.

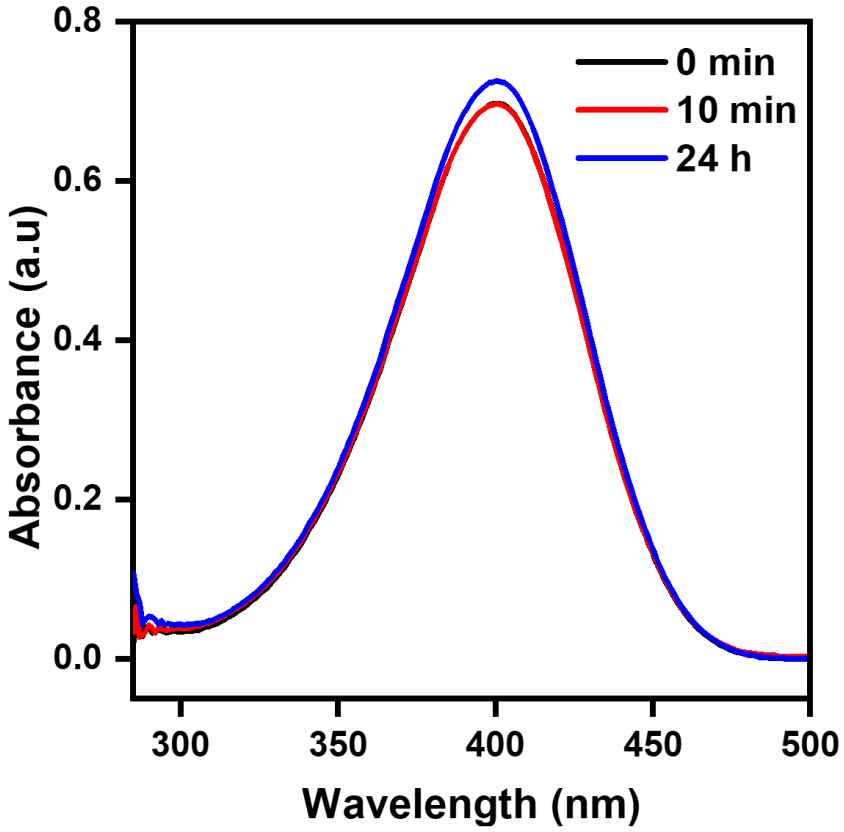

Figure 3.9: Time dependent UV–Vis spectra changes for the reduction of 4-NP using $NaBH_4$ in presence of capped SiO_2 NPs support.

3.7.3 Reduction of 4-Nitrophenol by Capped Ni-SiO_2 Nano-catalyst

Figure 3.10 illustrates the catalytic performance of the as prepared capped Ni-SiO_2 nano-catalysts. The catalytic activity of different mass ratios of capped Ni-SiO_2 (1:1, 1:2, and 1:3 mass ratio of Ni and SiO_2, respectively) nano-catalysts was investigated at various times dependent on UV-Vis's adsorption spectra changes of 4-NP shown in Figure 3.10 (a-c).

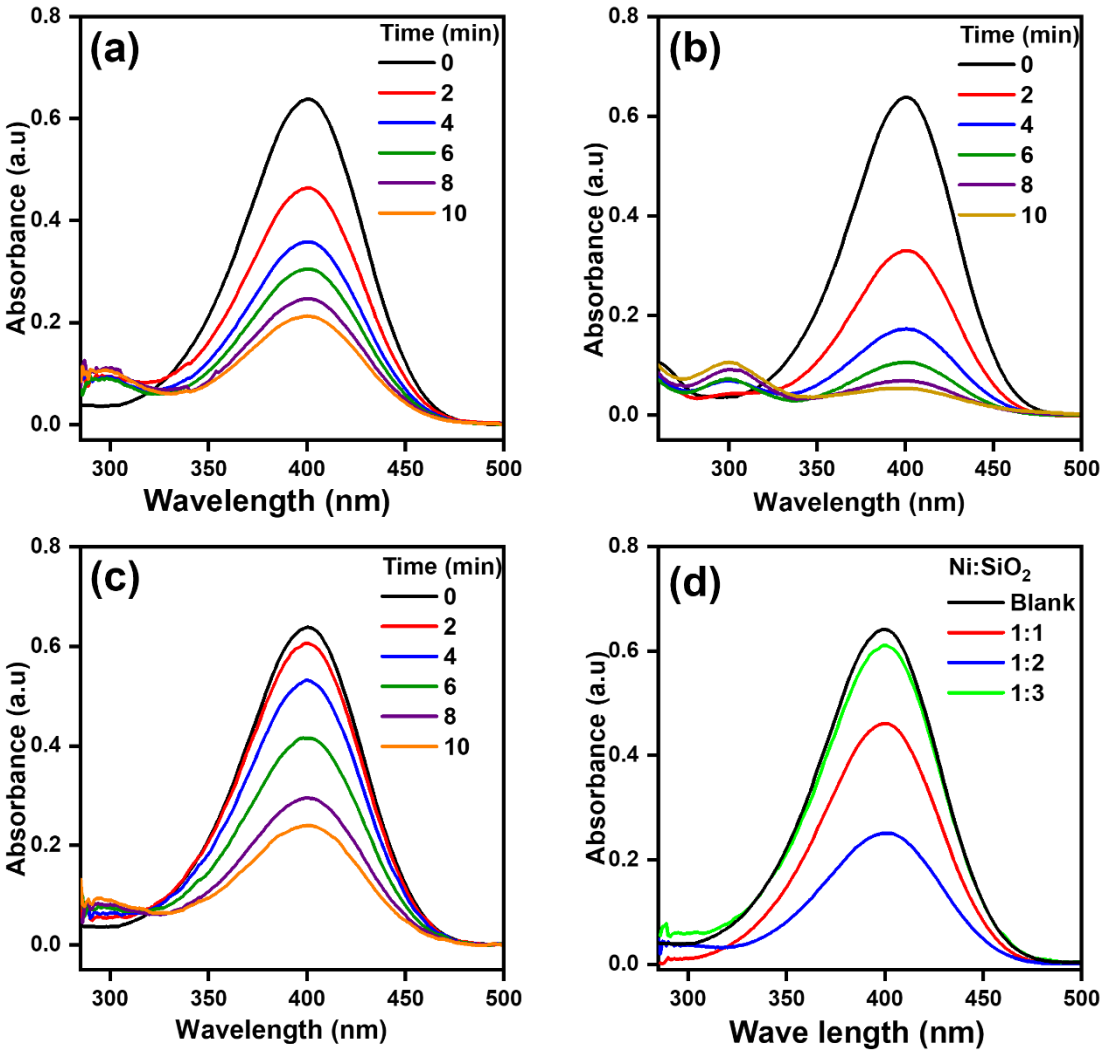

Figure 3.10: Time-dependent UV-vis spectral changes of the catalytic reduction of 4-NP to 4-AP using $NaBH_4$ in presence of capped Ni-SiO_2 nano-catalysts at different mass ratio of (a) 1:1, (b) 1:2, and (c) 1:3; (d) UV-Vis spectra at 2 min for (a), (b) and (c) for comparison.

It can be seen that after adding capped Ni-SiO_2 nano-catalyst to the solution of 4-NP and $NaBH_4$, the peak intensity at 400 nm was decreased rapidly over a while, and at the same time, with the production of 4-AP, a new absorption peak started to rise as a shoulder about 300 nm. Since the peak at 400 nm was much stronger than that at 300 nm, the concentrations of 4-NP ions were measured, and the progress or kinetics of the reaction were monitored by recording the absorbance at 400 nm. However, after adding catalyst the absorbance range at 400 nm progressively decreases with increasing reaction time, accompanied by a great number of bubbles, and the color of the solution gradually changes to colorless. The comparative catalytic reduction of 4-NP to 4-AP using different mass ratios (1:1, 1:2 and 1:3) of capped Ni-SiO_2 nano-catalysts are shows in Figure 3.10(d). Among these nano-catalysts, the capped Ni-SiO_2 (1:2) nano-catalyst demonstrated that the reaction was occurred within 10 minutes. Compared to other nano-catalysts of mass ratios, the capped Ni-SiO_2 (1:2) nano-catalyst demonstrated superior catalytic properties as illustrated in Figure 3.10(d).

3.7.4 Effect of Mass Loading of Capped Ni-SiO_2 (1:2) Nano-catalyst

The catalytic activity of different amounts (1-4 mg) of capped Ni-SiO_2 (1:2) nano-catalyst was also studied, and with the increase of amounts, the catalytic performance also increased as can be seen in Figure 3.11(a-d) which is general trend of catalyst.

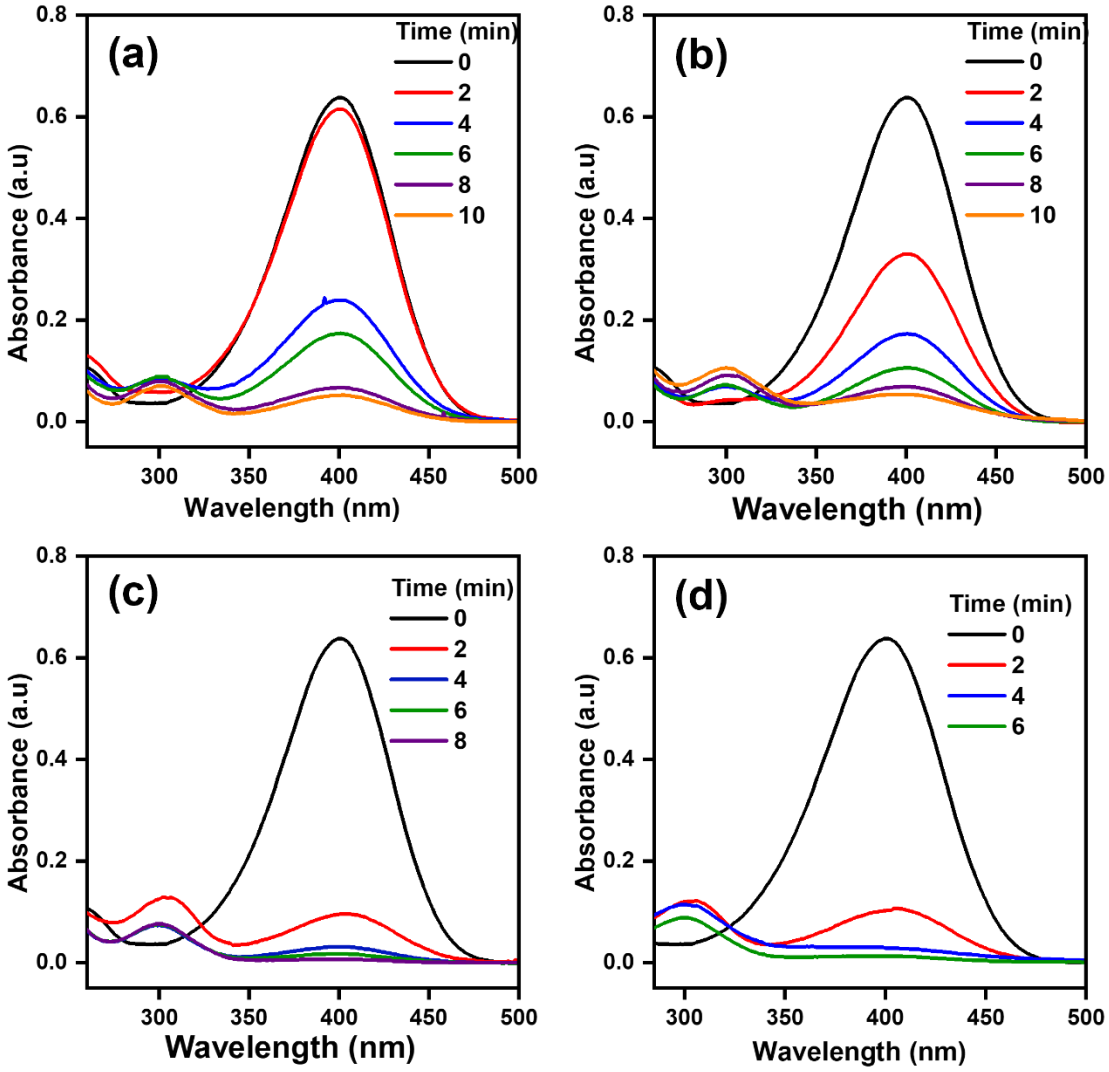

Figure 3.11: Time-dependent UV-vis spectral changes of the catalytic reduction of 4-NP to 4-AP using $NaBH_4$ at different amount of capped Ni-SiO_2 (1:2) nano-catalyst (a) 1 mg, (b) 2 mg, (c) 3 mg, and (d) 4 mg.

3.7.5 Kinetics for the Reduction of Nitroarenes

The kinetics of this reduction reaction was studied, which usually follows the pseudo-first-order kinetics concerning the concentration of 4-NP, utilized to compute the capped Ni-SiO_2 nano-catalyst's efficiency [28]. The reduction reaction was followed the pseudo-first-order kinetics because $NaBH_4$ was higher than 4-NP, and its concentration was maintained throughout the reduction reaction. The reaction rate constant, activity parameter, turnover frequency (TOF) can be described using the following Eq-3.1-3.3 [29].

$$\text{Ln}\frac{C_t}{C_0} = \ln\frac{A_t}{A_0} = -kt \qquad [3.1]$$

Where A_t and A_0 are the absorbance values at t = t and t = 0, rate constant k and the (C_t/C_0) value can be easily determined by measuring the relative absorption intensity (A_t/A_o), respectively.

$$\text{Activity Parameter (mg}^{-1}\text{ min}^{-1}\text{)} = k/M \qquad [3.2]$$

Where k is rate constant, M is amounts of catalysts used

$$\text{TOF (h}^{-1}\text{)} = \text{Turn over number/ time in hour} \qquad [3.3]$$

Table 3.3: Comparison of *k*, *K*, TOF of different nano-catalysts for the reduction of 4-NP

Catalyst	k (min^{-1})	Activity Parameter (mg^{-1} min^{-1})	R^2	TOF (h^{-1})	Conversion (%)
Ni-SiO_2 (1:1)	0.1078	0.1617	0.981	0.0271	66.72
Ni-SiO_2 (1:2)	0.2725	0.4087	0.994	0.1084	95.31
Ni-SiO_2 (1:3)	0.0980	0.1470	0.986	0.03	62.51

Figure 3.12(a) shows the relation of relative absorption intensity (A_t/A_0), as the relative concentration (C_t / C_0) with reduction time of 4-NP to 4-AP under the presence of capped Ni-SiO_2 (with mass ratio of Ni and SiO_2 of 1:2, 1:3, and 1:1) nano-catalysts. By plotting linear plots of ln (C_t /C_0) with time in the presence of different mass ratios of nano-catalysts, as shown in Figure 3.12(b), the *k* value may be estimated.

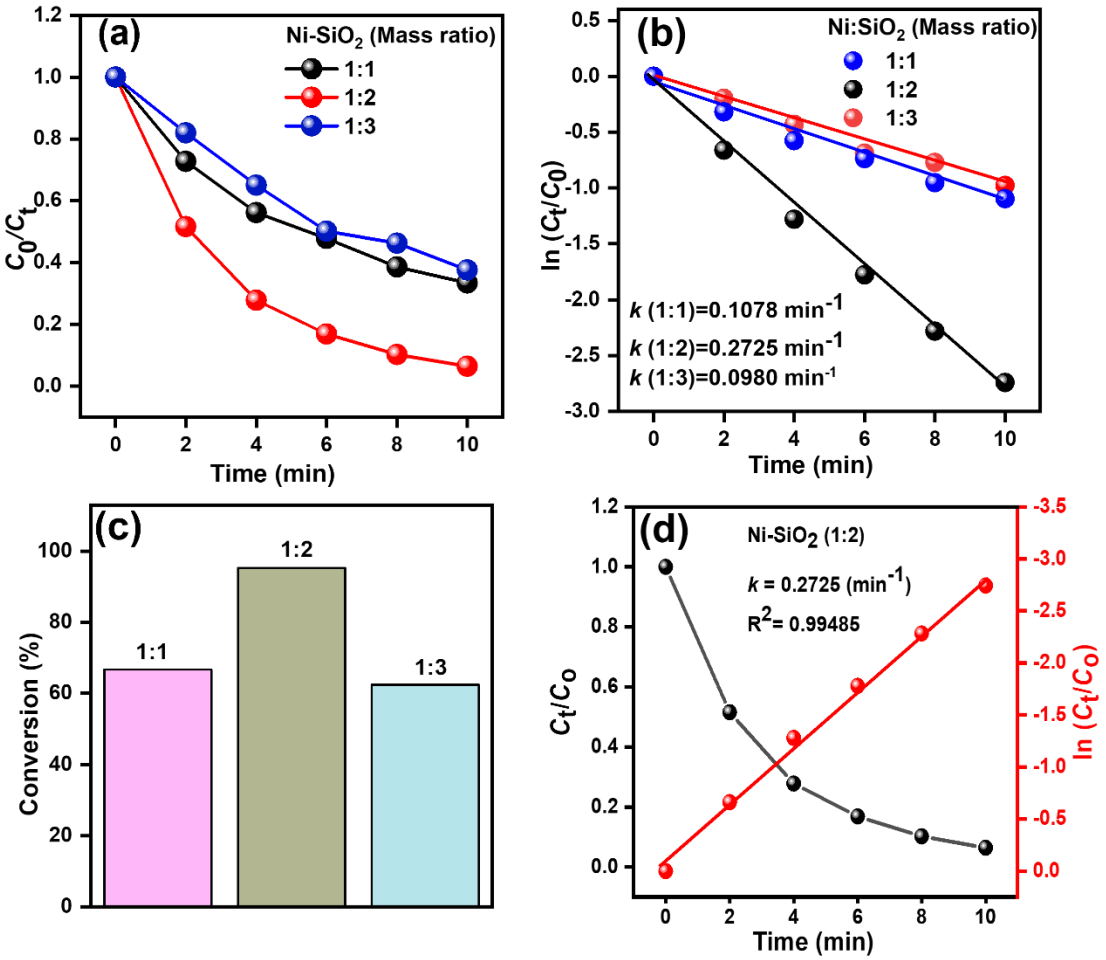

Figure 3.12: Pseudo-first-order kinetic data for the reduction reaction employed (a) plot (C_t/C_0) vs reaction time; (b) plot ln(C_t/C_0) vs time (c) relative conversion of 4-NP to 4-AP with different ratio capped Ni-SiO_2 nano-catalysts. (d) Comparative plot of (C_t/C_0) vs reaction time (black line), and ln (C_t/C_0) against the reaction time (red line) of 4-NP reduction with capped Ni-SiO_2 nano-catalyst at mass ratio of 1:2.

The ln (C_t / C_0) shows a strong linear correlation with reaction time for all catalysts, confirming the agreement with pseudo-first-order kinetics. The obtained rate constant *k*, activity parameter *K*, regression coefficient R^2, turnover frequency (TOF) and conversion (%) of the reduction of 4-NP to 4-AP with capped Ni-SiO_2 (with mass ratio of Ni and SiO_2 of 1:2, 1:3, and 1:1) nano-catalysts has been summarized in Table 3.3 the respective rate constant of all nano-catalysts are calculated to be 0.1078 min^{-1}, 0.2725 min^{-1} and 0.0980 min^{-1}, respectively. Among them the rate constant *k* of capped Ni-SiO_2 (1:2) nano-catalyst is 0.2725 min^{-1}, which is higher than the catalysts based on different mass ratios shows in Figure 3.12(d). The catalytic activity of the different

nano-catalysts follows the order of Ni-SiO_2 (1:3) < Ni-SiO_2 (1:1) < Ni-SiO_2 (1:2). Therefore, the performance of capped Ni-SiO_2 (1:2) nano-catalysts is higher than those of other nano-catalysts. The increasing amount of SiO_2 NPs in the catalyst decreases with the reduction reaction of the catalytic performance shows in Figure 3.12(a-c). On the other hand, the equal loading amount of SiO_2 and Ni NPs on the catalyst also decreases the catalytic activity, which had a significant agglomeration of Ni NPs, resulting in a low-rate constant. In order to illustrate the effect of mass ratio of the capped Ni-SiO_2 nano-catalyst, three column charts of mass ratio are compared Figure 3.12©. The conversion capability is shown in Figure 3.12.

Table 3.4: Comparison of *k*, *K* of different catalytic system for the reduction of 4-NP

Nano-Catalyst	Support surface	4-NP (mmol)	Catalyst (mg)	Time (min)	*k* (min^{-1})	K (min^{-1} mg^{-1})	References
Ni-SiO_2 (1:2)	**SiO_2**	**2×10^{-4}**	**2**	**10**	**0.2725**	**0.4087**	**Present work**
Au/ZSBA[a]-RD[b]	ZSBA	2.5×10^{-4}	10	15	0.1400	0.0140	[31]
Ag/PAN[c] CFN[d]	PAN	3×10^{-2}	10	70	0.0120	0.0012	[30]
RGO[e]/PtNi	RGO	5×10^{-3}	3	30	0.0672	0.0224	[32]
Ni NPs	None	3×10^{-4}	3	16	0.1600	0.0533	[33]
Pt-Au ANCs[f]	None	7×10^{-6}		33	0.0800		[34]

[a] Zeolite Socony Mobil–5/Santa Barbara Amorphous-15

[b]Rod

[c]Polyacrylonitrile

[d]Composite fibrous-networks

[e]Reduced Graphene Oxide

[f]Alloy nanocubes

To further demonstrate the superior catalytic performance of capped Ni-SiO_2 (1:2) nano-catalyst, a comparison of *k* and TOF between the as-prepared nano-catalyst and the catalysts reported in the literature are given in Table-3.4.

3.7.6 Recyclability Test of Capped Ni-SiO_2 Nano-catalyst

Catalytic reusability and stability are valuable characteristics for measuring the quality and practical applications of nano-catalysts [35, 36]. To evaluate the catalytic stability and reusability, the representative sample of capped Ni-SiO_2 (1:2) nano-catalyst was evaluated several cycles in reducing 4-NP by $NaBH_4$. After completion of the reaction process, the catalyst was recovered from the reaction mixture using an external magnet. Then the catalyst was washed with deionized water, and afterwards they were reused for the next cycle of the catalytic experiment without any drying of the used nano-catalysts. The recyclability of capped Ni-SiO_2 (1:2 mass ratio) nano-catalysts dependent on UV-Vis's adsorption spectra changes of 4-NP to 4-AP as are shown in Figures 3.13, 3.14 and 3.15. The obtained results exhibited that capped Ni-SiO_2 (1:2) nano-catalyst shows perfect recyclability at least for ten consecutive cycles without the significant loss of the catalytic activity as can be seen in Figure 3.16(a-c). The results of the reusability, plots of $\ln(C_t/C_0)$ vs time and the values of k for each cycle are shown in Figure 3.16(a, b). It shows that the k values slightly decrease with the increase in the number of cycles, and the errors are less than 10%.

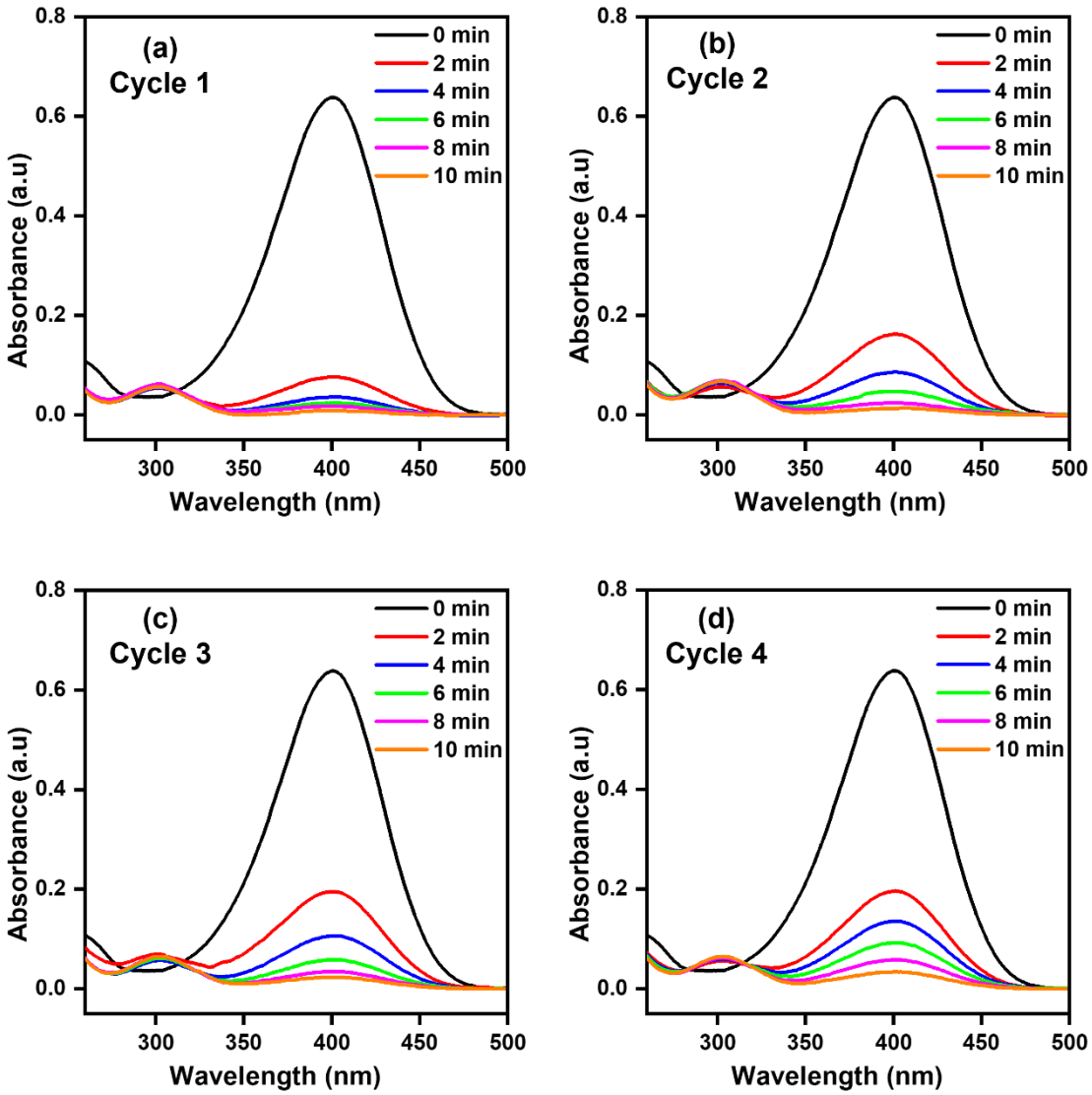

Figure 3.13: (a) UV-vis spectral changes during the catalytic reduction of 4-NP to 4-AP using $NaBH_4$ with capped Ni-SiO_2 (1:2) nano-catalyst up to 10 min. (b-d) each cycle corresponds the similar process like (a), but the catalyst was recycled in each case.

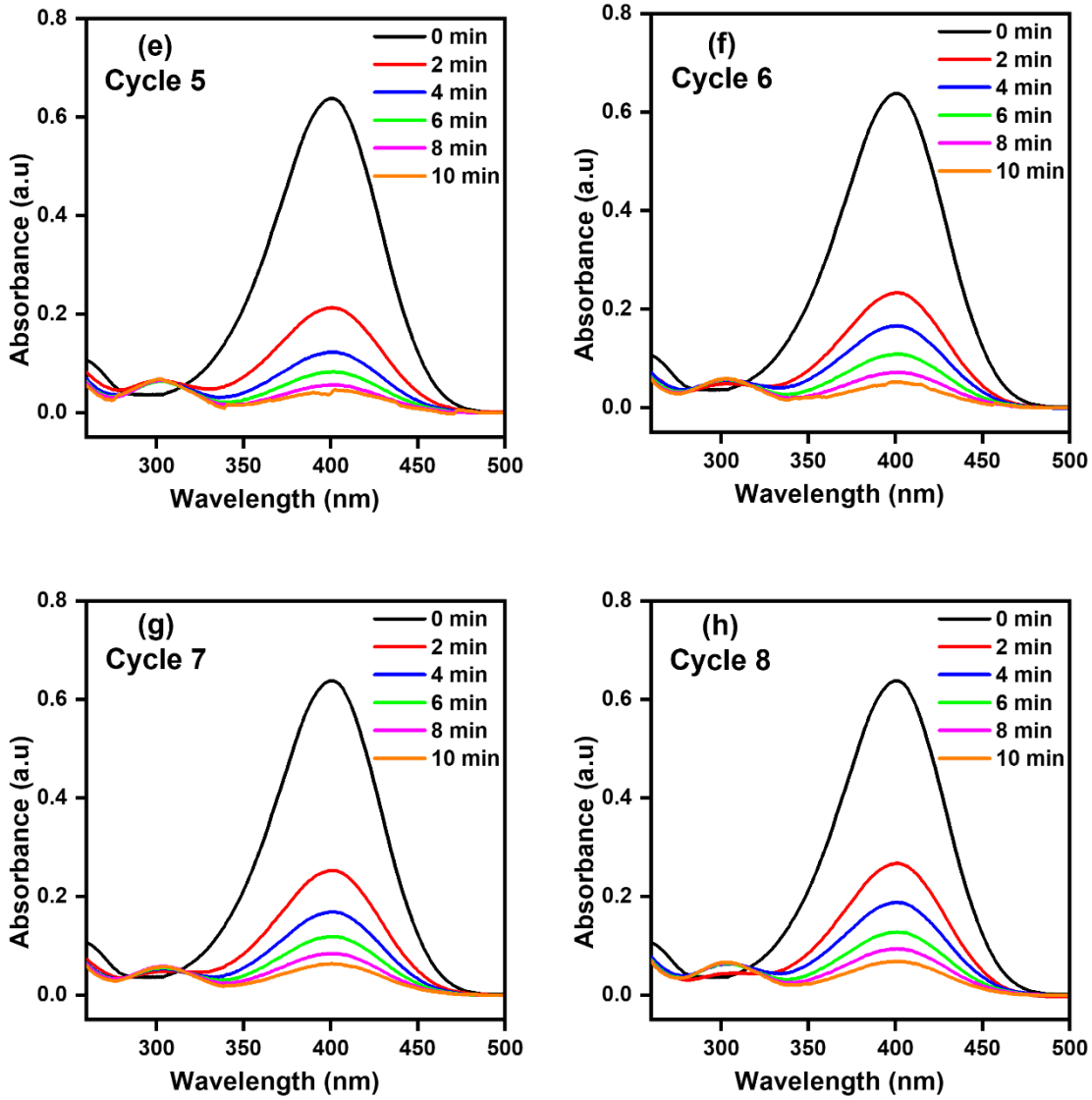

Figure 3.14: (e-h) each cycle corresponds the similar process like Fig 3.13(a), but the catalyst was recycled in each case.

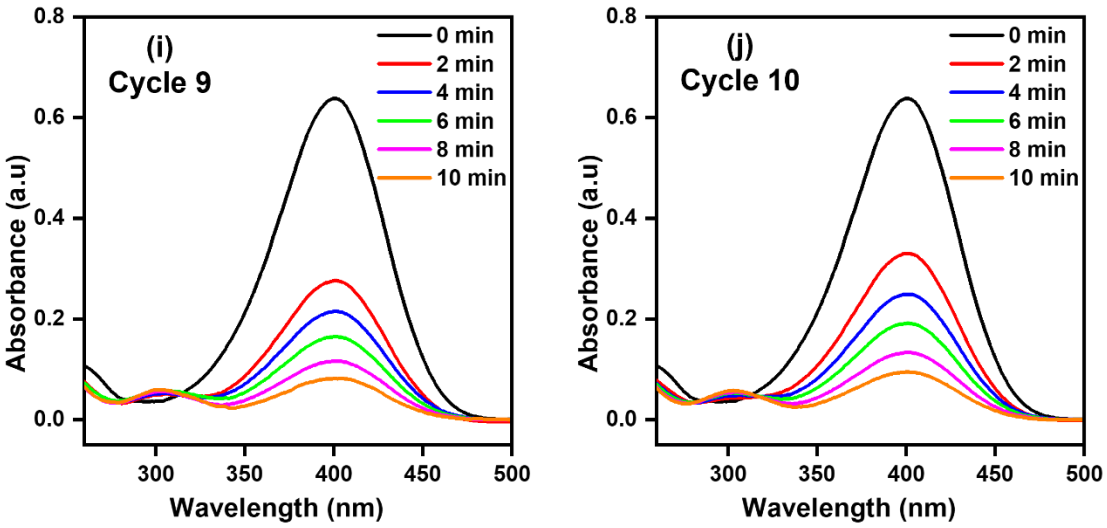

Figure 3.15: (i-j) each cycle corresponds the similar process like Fig 3.13(a), but the catalyst was recycled in each case.

It is found that the conversion remains higher than 89% even up to 10 cycles, indicating high stability. These consequences confirm that dispersion of Ni nanoparticles into porous SiO_2 nano surface with capping agent CTAB is easy to recycle and separate.

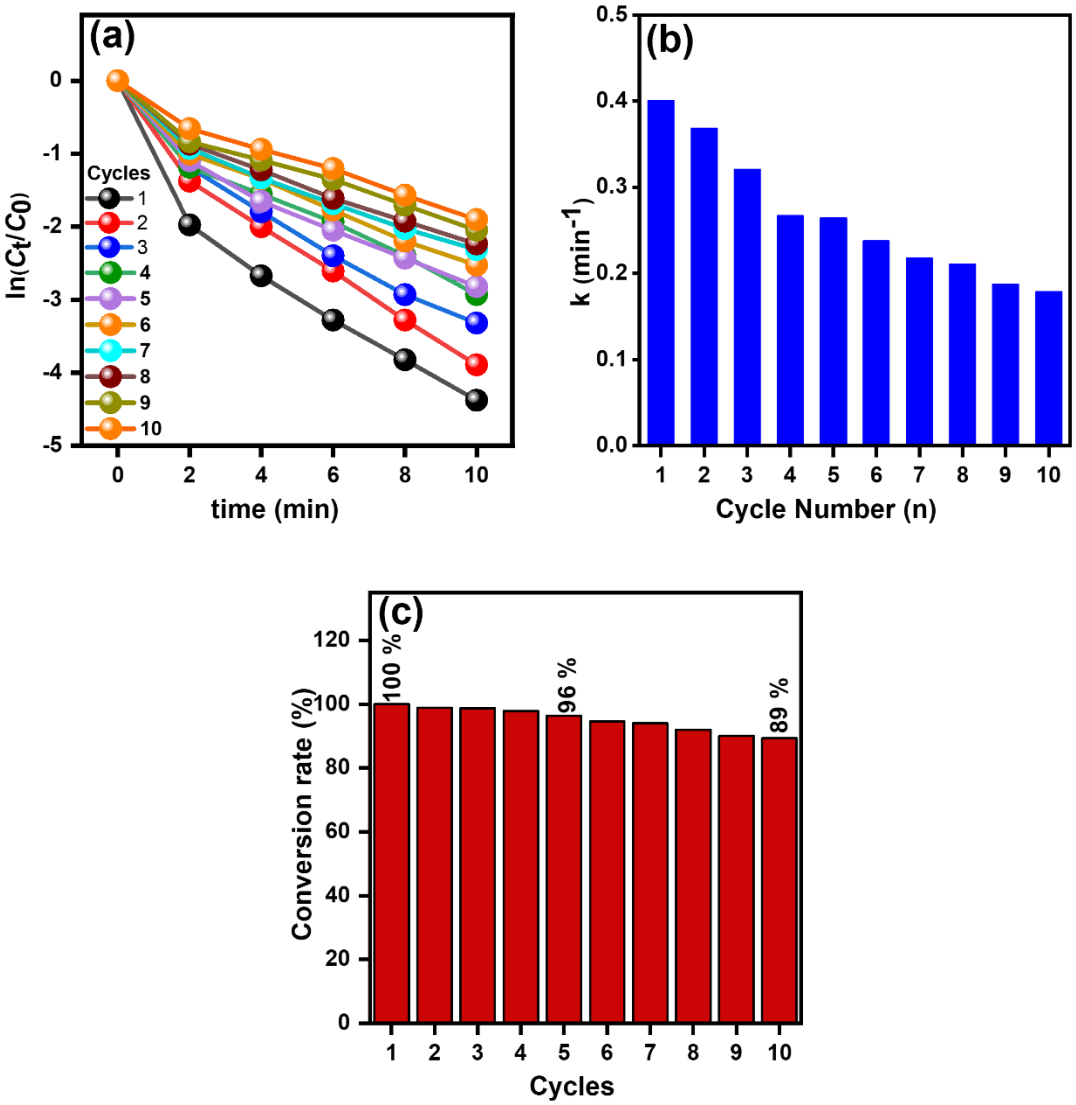

Figure 3.16: (a) The plots of ln (C_t/C_0) vs time and (b) the values of k vs cycles for different cycles in the recyclability test (c) Conversion rate at each cycle in the recyclability test.

The capped SiO_2 acted as a strong support and immobilized the Ni NPs in capped Ni-SiO_2 nano-catalyst which improve the catalytic stability of catalytic behavior of Ni NPs. The good stability is probably due to the unique in situ decomposition and reduction method, which leads to the tight assembly of Ni NPs on the silica support, which is hard to leach with repeated magnetic separation. As shown in Figure 3.16©, a slight decline in the conversion (< 4%) after 5 cycles and the average conversion was 95%.

3.7.7 Probable Mechanism of 4-NP reduction

Scheme 3.2 depicts the mechanism of catalytic reduction of 4-NP by capped Ni-SiO_2. In the presence of capped Ni-SiO_2, hydrogenation occurs. Furthermore, the capped SiO_2 practically never acts as a catalyst for the 4-NP reduction step. Only when immobilized Ni NPs are present on capped SiO_2 does the reaction conduct correctly. Furthermore, the capped Ni-SiO_2 is not the reactant.

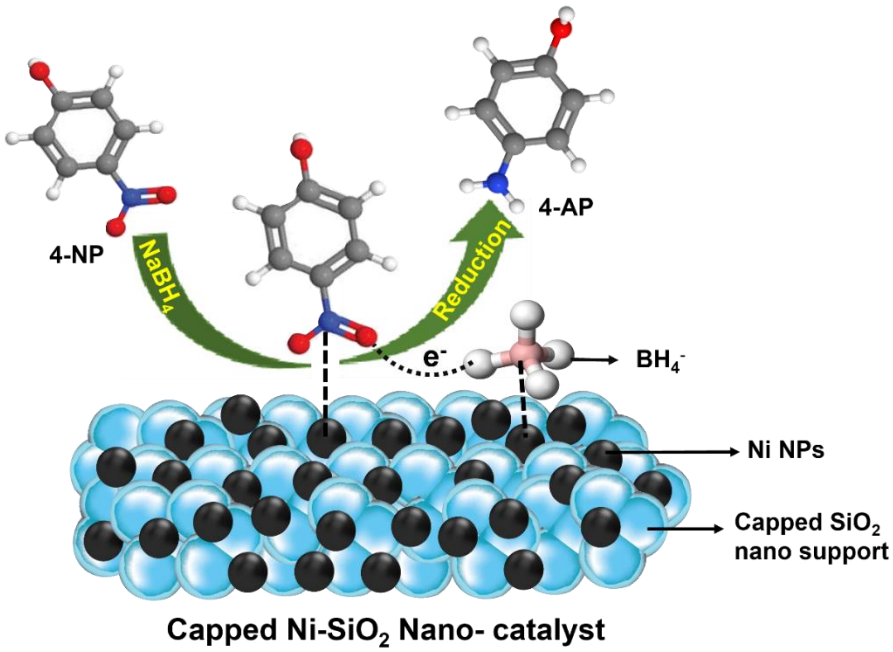

Scheme 3.2: Proposed mechanism of 4-NP reduction on the capped Ni-SiO_2 nano-catalyst by $NaBH_4$ in aqueous medium.

As a result, catalytic reduction takes place on the surface of immobilized Ni NPs of capped Ni-SiO_2. Based on the relevant literature, detailed information on the hydrogenation mechanism that occurs on the surface of metal NPs is proposed [37] [38]. The catalytic reduction process mainly consists of two parts: (1) The BH_4^- and 4-NP adsorb on the capped SiO_2 immobilized Ni NPs. Then, electron transfer and atomic exchange occur between BH_4^- and 4-NP, resulting in the formation of a new substance, 4-AP; (2) then, the 4-AP then continues to detach off the surface of the Ni NPs, exposing the active sites of the Ni NPs. Ni NPs play an important role in the reaction by providing several reaction sites for adsorption and lowering the kinetic energy barrier of the reduction. As a result, the capped Ni-SiO_2 nano-catalysts demonstrated excellent catalysis for the 4-NP to 4-AP reaction.

3.8 References

[1] Rovani, S., Santos, J. J., Corio, P., and Fungaro, D. A., "Highly Pure Silica Nanoparticles with High Adsorption Capacity Obtained from Sugarcane Waste Ash," *ACS Omega,* vol. 3, pp. 2618-2627, 2018.

[2] Alves, R. H., Reis, T. V. d. S., Rovani, S., and Fungaro, D. A., "Green Synthesis and Characterization of Biosilica Produced from Sugarcane Waste Ash," *J. Chem.,* vol. 2017, pp. 1-9, 2017.

[3] U. Kalapathy , A. P., J. Shultz, "A Simple Method for Production of Pure Silica from Rice Hull Ash," *Bioresour. Technol.,* vol. 73, pp. 257-262, 2000.

[4] Lin, H. P. and Mou, C. Y., "Structural and Morphological Control of Cationic Surfactant-Templated Mesoporous Silica," *Acc. Chem. Res.,* vol. 35, pp. 927-35, 2002.

[5] Sharma, R. K., Sharma, S., Dutta, S., Zboril, R., and Gawande, M. B., "Silica-Nanosphere-Based Organic–Inorganic Hybrid Nanomaterials: Synthesis, Functionalization and Applications in Catalysis," *Green Chemistry,* vol. 17, pp. 3207-3230, 2015.

[6] Wang, X., Li, W., Zhu, G., Qiu, S., Zhao, D., and Zhong, B., "Effects of Ammonia/Silica Molar Ratio on the Synthesis and Structure of Bimodal Mesopore Silica Xerogel," *Microporous Mesoporous Mater.,* vol. 71, pp. 87-97, 2004.

[7] Wu, S. H., Mou, C. Y., and Lin, H. P., "Synthesis of Mesoporous Silica Nanoparticles," *Chem. Soc. Rev.,* vol. 42, pp. 3862-75, 2013.

[8] Hoffmann, F., Cornelius, M., Morell, J., and Froba, M., "Silica-Based Mesoporous Organic-Inorganic Hybrid Materials," *Angew. Chem. Int. Ed. Engl.,* vol. 45, pp. 3216-51, 2006.

[9] Li, W., Xiao, F., Su, H., Wang, D., and Yang, X., "Investigation of Adsorption and Photocatalytic Activities of in Situ Cetyltrimethylammonium Bromide-Modified Bi/Biocl Heterojunction Photocatalyst for Organic Contaminants Removal," *RSC Adv.,* vol. 6, pp. 93309-93317, 2016.

[10] Neouze, M.-A. and Schubert, U., "Surface Modification and Functionalization of Metal and Metal Oxide Nanoparticles by Organic Ligands," *Monatsh. Chem.,* vol. 139, pp. 183-195, 2008.

[11] Guan, H., Chao, C., Lu, Y., Shang, H., Zhao, Y., Yuan, S., and Zhang, B., "Ptni Nanoparticles Embedded in Porous Silica Microspheres as Highly Active Catalysts for P-Nitrophenol Hydrogenation to P-Aminophenol," *J. Chem. Sci.*, vol. 128, pp. 1355-1365, 2016.

[12] Nicholls, D. and Swindells, R., "Hydrazine Complexes of Nickel(II) Chloride," *J. Inorg. Nucl. Chem.*, vol. 30, pp. 2211-2217, 1968.

[13] Araichimani, P., Suresh Kumar, G., Prabu, K. M., Karunakaran, G., Van Minh, N., Kolesnikov, E., and Gorshenkov, M. V., "Amorphous Silica Nanoparticles Derived from Biowaste Via Microwave Combustion for Drug Delivery," *Inter. J. Appl. Cer.Techn.*, vol. 18, pp. 583-589, 2021.

[14] Boudjahem, A. G., Monteverdi, S., Mercy, M., and Bettahar, M. M., "Study of Support Effects on the Reduction of Ni^{2+} Ions in Aqueous Hydrazine," *Langmuir*, vol. 20, pp. 208-13, 2004.

[15] Jinzhang Gao, F. G., Yanchun Zhao, Wu Yang, Yongjun Ma, Xiaoquan Lu, Jingguo Hou, Jingwan Kang, "Preparation of Ultrafine Nickel Powder and Its Catalytic Dehydrogenation Activity," *Mater. Chem. Phys.*, vol. 71, pp. 215-219, 2001.

[16] Arun Kumar, D., Merline Shyla, J., and Xavier, F. P., "Synthesis and Characterization of TiO_2/SiO_2 Nano Composites for Solar Cell Applications," *Appl. Nanosci.*, vol. 2, pp. 429-436, 2012.

[17] Zhang, T., Xu, G., Puckette, J., and Blum, F. D., "Effect of Silica on the Structure of Cetyltrimethylammonium Bromide," *J. Phys. Chem. C*, vol. 116, pp. 11626-11634, 2012.

[18] Ruiz, Y. P., Ferrão, M. F., Cardoso, M. B., Moncada, E. A., and dos Santos, J. H. Z., "Structural Discrimination of Nanosilica Particles and Mixed-Structure Silica by Multivariate Analysis Applied to SAXS Profiles in Combination with FT-IR Spectroscopy," *RSC Adv.*, vol. 6, pp. 72306-72316, 2016.

[19] Zamiranvari, A., Solati, E., and Dorranian, D., "Effect of Ctab Concentration on the Properties of Graphene Nanosheet Produced by Laser Ablation," *Opt. Laser Technol.*, vol. 97, pp. 209-218, 2017.

[20] Rodríguez-Díaz, J. M., García, J. O. P., Sánchez, L. R. B., da Silva, M. G. C., da Silva, V. L., and Arteaga-Pérez, L. E., "Comprehensive Characterization of Sugarcane Bagasse Ash for Its Use as an Adsorbent," *BioEnergy Research*, vol. 8, pp. 1885-1895, 2015.

[21] Bm, V. and M, V., "Photocatalytic Degradation of Toxic Methyl Red Dye Using Silica Nanoparticles Synthesized from Rice Husk Ash," *J Environ. Anal. Toxicol.*, vol. 05, 2015.

[22] Chen, F. *et al.*, "Organosilica Nanoparticles with an Intrinsic Secondary Amine: An Efficient and Reusable Adsorbent for Dyes," *ACS Appl. Mater. Interfaces,* vol. 9, pp. 15566-15576, 2017.

[23] Chen, X., Jiang, J., Yan, F., Tian, S., and Li, K., "A Novel Low Temperature Vapor Phase Hydrolysis Method for the Production of Nano-Structured Silica Materials Using Silicon Tetrachloride," *RSC Adv.*, vol. 4, 2014.

[24] Wu, X., Xing, W., Zhang, L., Zhuo, S., Zhou, J., Wang, G., and Qiao, S., "Nickel Nanoparticles Prepared by Hydrazine Hydrate Reduction and Their Application in Supercapacitor," *Powder Technol.*, vol. 224, pp. 162-167, 2012.

[25] Wang, R., Wu, K., and Wu, C., "Highly Sensitive Electrochemical Detection of Bisphenol a Based on the Cooperative Enhancement Effect of the Graphene–$Ni(OH)_2$ Hybrid and Hexadecyltrimethylammonium Bromide," *Analytical Methods,* vol. 7, pp. 9261-9267, 2015.

[26] Ming, M., Zhang, Y., He, C., Zhao, L., Niu, S., Fan, G., and Hu, J. S., "Room-Temperature Sustainable Synthesis of Selected Platinum Group Metal (PGM = Ir, Rh, and Ru) Nanocatalysts Well-Dispersed on Porous Carbon for Efficient Hydrogen Evolution and Oxidation," *Small,* vol. 15, pp. e1903057, 2019.

[27] Zhang, K., Suh, J. M., Choi, J. W., Jang, H. W., Shokouhimehr, M., and Varma, R. S., "Recent Advances in the Nanocatalysts-Assisted $NaBH_4$ Reduction of Nitroaromatics in Water," *ACS Omega,* vol. 4, pp. 483-495, 2019.

[28] Zeng, J., Zhang, Q., Chen, J., and Xia, Y., "A Comparison Study of the Catalytic Properties of Au-Based Nanocages, Nanoboxes, and Nanoparticles," *Nano Lett.*, vol. 10, pp. 30-5, 2010.

[29] Wu, M., Li, Y., Yue, R., Zhang, X., and Huang, Y., "Removal of Silver Nanoparticles by Mussel-Inspired Fe_3O_4@Polydopamine Core-Shell Microspheres and Its Use as Efficient Catalyst for Methylene Blue Reduction," *Sci Rep,* vol. 7, pp. 42773, 2017.

[30] Gao, S., Zhang, Z., Liu, K., and Dong, B., "Direct Evidence of Plasmonic Enhancement on Catalytic Reduction of 4-Nitrophenol over Silver Nanoparticles Supported on Flexible Fibrous Networks," *Appl. Catal. B,* vol. 188, pp. 245-252, 2016.

[31] Gao, D. *et al.*, "Morphology-Selective Synthesis of Active and Durable Gold Catalysts with High Catalytic Performance in the Reduction of 4-Nitrophenol," *Nano Research*, vol. 9, pp. 3099-3115, 2016.

[32] Sahoo, P. K., Panigrahy, B., and Bahadur, D., "Facile Synthesis of Reduced Graphene Oxide/Pt–Ni Nanocatalysts: Their Magnetic and Catalytic Properties," *RSC Adv.*, vol. 4, pp. 48563-48571, 2014.

[33] Jiang, Z., Xie, J., Jiang, D., Wei, X., and Chen, M., "Modifiers-Assisted Formation of Nickel Nanoparticles and Their Catalytic Application to P-Nitrophenol Reduction," *CrystEngComm*, vol. 15, pp. 560-569, 2013.

[34] Fu, G., Ding, L., Chen, Y., Lin, J., Tang, Y., and Lu, T., "Facile Water-Based Synthesis and Catalytic Properties of Platinum–Gold Alloy Nanocubes," *CrystEngComm*, vol. 16, pp. 1606-1610, 2014.

[35] Jana, D., Dandapat, A., and De, G., "Anisotropic Gold Nanoparticle Doped Mesoporous Boehmite Films and Their Use as Reusable Catalysts in Electron Transfer Reactions," *Langmuir*, vol. 26, pp. 12177-84, 2010.

[36] Lin, F.-h. and Doong, R.-a., "Bifunctional Au−Fe_3O_4 Heterostructures for Magnetically Recyclable Catalysis of Nitrophenol Reduction," *J. Phys. Chem. C*, vol. 115, pp. 6591-6598, 2011.

[37] Liu, L., Chen, R., Liu, W., Wu, J., and Gao, D., "Catalytic Reduction of 4-Nitrophenol over Ni-Pd Nanodimers Supported on Nitrogen-Doped Reduced Graphene Oxide," *J. Hazard. Mater.*, vol. 320, pp. 96-104, 2016.

[38] Xu, Z., He, X., Liang, M., Sun, L., Li, D., Xie, K., and Liao, L., "Catalytic Reduction of 4-Nitrophenol over Graphene Supported Cu@Ni Bimetallic Nanowires," *Mater. Chem. Phys.*, vol. 227, pp. 64-71, 2019.

Chapter-4

Conclusions

4. Conclusions

Capped SiO_2 NPs as an excellent support surface was successfully prepared from SCB bio-waste. Ni NPs was immobilized with well dispersion on that support capped SiO_2 NPs using CTAB, a stabilizer and size controller. The agglomeration and low activity of Ni NPs was completely resolved by using this support surface and capping agent. In addition, FESEM, EDX, FTIR, and XRD methods were effectively used to verify the morphological, structural, and compositional aspects of the capped Ni-SiO_2 nano-catalyst. The catalytic activity of the prepared three nanostructured capped Ni-SiO_2 (1:1, 1:2, and 1:3) nano-catalysts was investigated towards reduction of 4-NP to 4-AP with the excess amounts of $NaBH_4$ in water. The unique and well-dispersed capped Ni-SiO_2 (1:2) nano-catalyst showed high activity and a good catalytic performance. The borohydride reduction of 4-NP with capped Ni-SiO_2 nano-catalysts was obeyed by the kinetics of pseudo-first order. The capped Ni-SiO_2 (1:2) nano-catalyst demonstrated superior catalytic activity (TOF of 0.1084 h^{-1}) and could convert 4-NP to 4-AP within 10 min. The nano-catalyst also showed outstanding recyclability and reduction efficiency, as well as 89% conversion even after ten cycles. The capped Ni-SiO_2 nano-catalyst can be used as an effective and reusable catalyst for practical applications with eco-friendliness, easy for recycle and markedly cost-effectiveness. The method of CTAB capping adopted was efficient enough to result a well dispersed immobilization Ni NPs into the capped SiO_2 NPs support. The synthetic strategy provides a useful idea for a controllable synthesis and immobilization pathways of metal NPs.